Chapter 1

Relativistic Nucleus-Nucleus Collision – an Overview

1.1 Introduction

QCD is the quantum field theory of strong interaction. The theory describes how partons (quarks and gluons), the fundamental constituents of all strongly interacting particles, namely the hadrons (which also include the nucleons), interact with each other. The idea of color degree of freedom plays an important role in strong interaction. Quarks carry three varieties of color, while all hadrons must be color neutral (singlet) composite objects in the same sense as all atoms are electrically neutral. The quarks interact with each other by exchanging gluons, the quanta of strong interaction, which themselves are color carrying objects. Unlike atoms the hadrons are guided by a phenomenon called the *asymptotic freedom* [1, 2], the basic essence of which is that the QCD interaction strongly depends on the length scale. For two colored particles the interaction is strong at large and weak at small separations. As a result, the partons are permanently confined within hadrons, and till date nobody has been able to isolate a quark. Fig. 1.1 shows how the QCD *running coupling constant* α_s varies with the momentum transfer Q [3]. Small values of α_s correspond to a large momentum transfer or equivalently a short distance when the partons are weakly interacting. Under such a situation the confinement phenomenon can be explained

in terms of a perturbative QCD (pQCD). On the other hand, at a low momentum transfer or equivalently at a large distance α_s is large, and the strongly coupled QCD state becomes highly nonperturbative. In the ideal QCD Lagrangian quarks are considered as massless point particles. However, a quark confined within a hadron can polarize the surrounding gluon field and acquire a dynamically generated effective mass, also known as the *constituent* mass, whose typical value for light quarks is about 350 MeV in baryons and slightly less in mesons [4]. The process of mass acquisition by fundamental particles like quarks and leptons, is largely (about 98%) due to spontaneous breaking of chiral symmetry and marginally (about 2%) due to the interaction with the Higgs field. A fascinating consequence of the idea of asymptotic freedom was recognized shortly after it was introduced. If the normal nuclear matter can be subjected to extremely high values of temperature and pressure, it becomes difficult for the constituent partons to remain within the confinements of individual color neutral hadrons. Under such circumstances the parton-parton coupling becomes loose while the quarks and gluons can move freely over a region that can perhaps be wider than the hadronic dimension ($\sim$ 1 fm.) at least by an order [5]. If the temperature is raised to a sufficiently high value say $T > 100\,\mathrm{GeV}$: $(1\,\mathrm{MeV} \approx 10^{10}\,K)$, the gluonic cloud surrounding the quarks will melt down, thereby restoring the chiral symmetry. At vanishing baryon density deconfinement and chiral symmetry restoration may take place simultaneously, while at high baryon density the former probably precedes the latter [6]. A color conducting deconfined state of weakly interacting partons comes as a solution of pQCD. A state similar to this perhaps filled up our entire universe at the very early stages of its creation–from the time of electro-weak decoupling (a few pico-secs) to hadronization (several micro-secs) after the *Big bang*. However, the highest limiting temperature at which a state of color neutral hadrons can survive is set at a much smaller value ($T \approx 170\,\mathrm{MeV}$) [7]. Therefore, a confinement–deconfinement transition is possible even at a much lower temperature. Corresponding deconfined state may however not be so weakly coupled and needs to be treated non-perturbatively. In a different approach nuclear matter is squeezed so hard that a large number of constituent (valence) quarks are compelled to assemble in the close proximity of every other single quark, and none of them can anymore recognize which other quark(s) did it partner with in the original nucleon. Such a situation may also lead to the formation of a color conducting deconfined state at a much lower temperature but at a higher baryo-chemical potential ($\mu_B \sim$ several hundred MeV). A similar state perhaps forms the core of very compact astrophysical objects like the neutron stars, which having temperatures $T \sim 10^5 - 10^9$ K may be considered as cold in the partonic scale [8].

When two heavy nuclei with high incoming energies are allowed to impinge upon each other, a central 'fireball' is created. Depending purely on the initial conditions a local thermal and/or chemical equilibrium may be achieved. Under favorable thermodynamic conditions such an equilibrated state may undergo a transition from a state of interacting

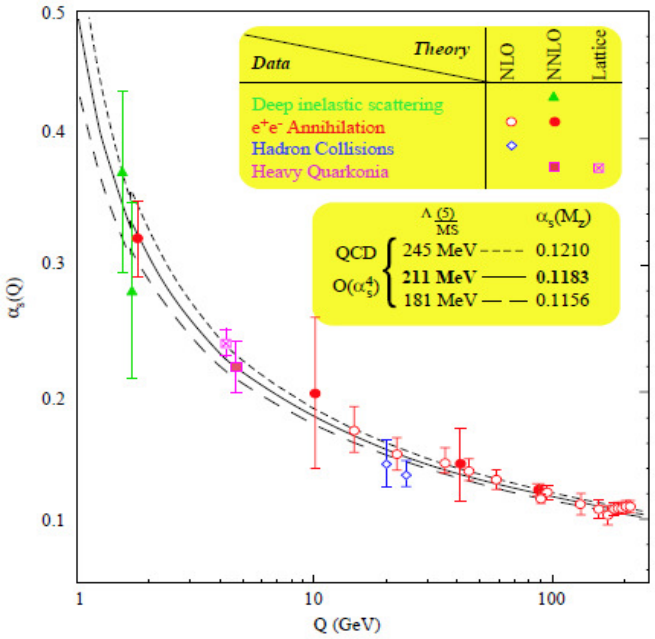

Figure 1.1: Summary of measurements of $\alpha_s(Q)$. The curves shown differ in their choice of the QCD scale parameter Λ_{QCD} [3].

nucleons to a color conducting state called the *Quark-gluon Plasma* (QGP) [5, 9, 10], where deconfined quarks and gluons can propagate over nuclear rather than merely nucleonic volumes. As indicated above, through AB interactions it is possible to recreate the initial evolutionary stages of our universe since it came into being, or to produce the state of matter similar to what probably fills up the core of very compact astrophysical objects, states that are otherwise experimentally inaccessible in every possible sense. The science of small elementary particles is therefore, deeply intertwined with the science of the large, the study of the origin and the evolution of the universe. Fig. 1.2 shows a schematic of the temperature history of our universe as it evolved with time after its creation [11]. At times $\sim 10\,\mu$sec. after the Big bang, at temperature $T \sim 200$ MeV the universe was in the state of QGP. In present-day experiments by colliding two heavy-ions at relativistic energies, we may try to recreate that kind of matter in the laboratory through a *Little bang*. One has to remember that any such terrestrially created fireball will certainly contain much less energy, and will be much shorter lived ($\sim 10^{-22}$ sec.) than the primordial one. As the infant universe expanded and cooled down, the plasma phase of matter went through a transition to form a variety of particles, most importantly the nucleons which constitute different forms of matter as we see them today. However, unless the system under consideration behaves like matter and not like individual particles or a group of particles, it is inappropriate to discuss the same in terms of phase transition or local equilibrium. A local equilibrium means that the lifetime of the fireball must be significantly larger than the inverse rate of binary collisions taking place within it. Each constituent particle should experience at least several collisions. It is also

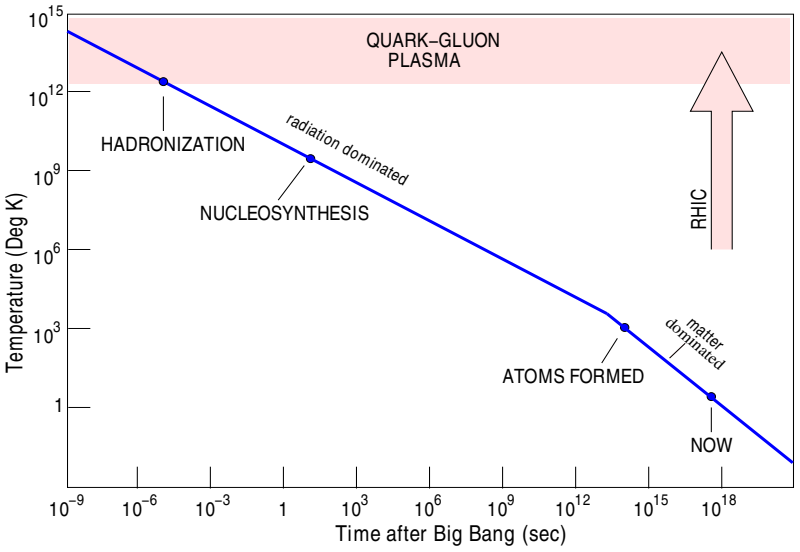

Figure 1.2: Temperature history of the universe–from Big Bang to Little Bang.

necessary to establish that the non-hadronic degrees of freedom present in the fireball form a statistical ensemble, so that concepts like temperature, chemical potential and flow velocity can be applied to the system, and the system can be characterized by an experimentally determinable equation of state. The measurements should further enable us to determine the physical characteristics of phase transition like its order, the critical temperature and the speed of sound in hadronic/partonic medium along with the nature of quasi-particle states [12]. For two reasons an interacting AB system is better suited than a proton-proton (pp) system in this regard. First, in a high-energy AB collision at the same incident energy per nucleon, the average multiplicity of the newly produced particles is much higher (as large as 10^4 per event at the highest possible collision energy achieved till date) than that of a pp collision. Thus the relative fluctuations of thermodynamic parameters that are usually required to characterize a state, will be less. Second, in the AB system there will be many rescattering among the nucleons of the colliding nuclei so that enough spacetime is available before a local equilibrium settles down within the radiation and matter mix-up prevailing in the central reaction zone, so that the same can be called 'a state' [13].

1.2 Relativistic Kinematics

High-energy interactions between particles should be studied by using such kinematic variables that have simple transformation properties as we move from one Lorentz frame to the other. The distribution functions plotted in terms of such variables in one frame of reference can then be very easily redrawn in another Lorentz transformed frame. Conventionally in a fixed target experiment measurements are made in the laboratory system (LS), and in a

collider experiment in the CM system (CMS) which for a symmetric (AA) collision coincides with the LS. Some of the commonly used kinematic variables in high-energy collisions are introduced below.

• **Energy in LS and CMS:** For a target fixed in the LS, the projectile (rest mass m_1 and incident energy E_1) and the target (rest mass m_2) four momenta may, respectively be denoted by:

$$p_1 = (E_1,\, \boldsymbol{p_1}) \qquad \text{and} \qquad p_2 = (m_2,\, \mathbf{0}) \tag{1.1}$$

the relativistic energy-momentum relation being effective for each particle. In the CMS both will have equal and opposite three momenta. Corresponding four momenta will be:

$$p_1^* = \left(E_1^*,\, \boldsymbol{p_1^*}\right) \qquad \text{and} \qquad p_2^* = \left(E_2^*,\, \boldsymbol{p_2} = -\boldsymbol{p_1^*}\right). \tag{1.2}$$

In the CMS the total four momenta (s) of the colliding system is

$$(p_1^* + p_2^*)^2 = (E_1^* + E_2^*)^2 \,-\, \left(\boldsymbol{p_1^*} + \boldsymbol{p_2^*}\right)^2 = (E_1^* + E_2^*)^2 = E_{cm}^2 \equiv s. \tag{1.3}$$

Therefore, $\sqrt{s}$ denotes the total energy available in the CMS which is also called the invariant mass of the CMS. On the other hand in LS

$$(p_1 + p_2)^2 = (E_1 + m_2)^2 - \boldsymbol{p_1}^2 = m_1^2 + m_2^2 + 2\, m_2\, E_1. \tag{1.4}$$

Therefore, using Lorentz invariance of $\sqrt{s}$ one can write,

$$E_{cm} = \sqrt{s} = \sqrt{m_1^2 + m_2^2 + 2\, m_2\, E_1} \tag{1.5}$$

In the LS the CMS moves in the direction of $\boldsymbol{p_1}$ with a Lorentz factor,

$$\gamma_{cm} = \frac{E_1 + m_2}{\sqrt{s}} \qquad \Rightarrow \quad \sqrt{s} = \frac{E_{lab}}{\gamma_{cm}} \tag{1.6}$$

In a collider experiment if the incident energies are very high ($E_1,\, E_2 >> m_1,\, m_2$),

$$E_{cm}^2 \approx 4\, E_1\, E_2 \qquad \Rightarrow \quad E_{cm} \approx 2E$$

when $E_1 = E_2 = E$ say. Under a similar situation, $E_{cm} \approx \sqrt{2\, m_2\, E_1}$ for a fixed target experiment. For a symmetric AA collision the total CM energy is related to the CM energy of an NN system ($\sqrt{s}_{NN}$) by, $\sqrt{s} = A\sqrt{s}_{NN}$ with a Lorentz factor

$$\gamma_{cm} = \frac{E}{M} = \frac{\sqrt{s}}{2A\, m_N} = \frac{\sqrt{s}_{NN}}{2m_N}, \tag{1.7}$$

where m_N is the mass of a nucleon. For asymmetric collisions however, it is difficult to fix the 'effective' CM frame which is dependent on the impact parameter of the collision. Therefore, the number of participating and spectator nucleons need to be determined first, posing extra problems particularly for soft processes. For hard processes that are more likely to be observed in central collisions, the NN frame still works.

• **Transverse Momentum:** The *transverse momentum* ($\boldsymbol{p}_{_\perp}$) of a particle is the momentum component in a direction perpendicular to the beam direction. Obviously $\boldsymbol{p}_{_\perp}$ is related to the longitudinal component $p_{_L}$ as $|\boldsymbol{p}| = \sqrt{\boldsymbol{p}_\perp^2 + p_{_L}^2}$. One can define the *transverse mass* ($m_{_\perp}$) through $m_{_\perp} = \sqrt{\boldsymbol{p}_\perp^2 + m^2}$, where m is the rest mass of the particle. The azimuthal angle (φ), defined over the transverse plane is introduced as, $\varphi = \tan^{-1}(p_y/p_x)$.

• **Rapidity Variable:** The *rapidity variable* (y), parameter of the 'Lorentz boost', can either be defined in terms of the energy-momentum components (E, $\boldsymbol{p}$) or in terms of the space-time components ($t, \mathbf{x}$) of a particle as,

$$y = \frac{1}{2}\ln\left(\frac{E + p_{_L}}{E - p_{_L}}\right) \qquad \text{or} \qquad y = \frac{1}{2}\ln\left(\frac{t+z}{t-z}\right) \tag{1.8}$$

Here $p_{_L}$ is the longitudinal component of the momentum and z is the space co-ordinate of a particle along the beam direction. y is a dimensionless quantity related to the ratio of the forward light-cone momentum ($p_{_+}$) to the backward light-cone momentum ($p_{_-}$) of the particle, can either be positive or negative. In the nonrelativistic limit, the rapidity of a particle traveling along the longitudinal direction is equal to the velocity of the particle in the unit of velocity of light in vacuum. One can easily show that, $E = m_{_\perp}\cosh y$ and $p_{_L} = m_{_\perp}\sinh y$. The energy and momentum of the CMS in the LS, respectively are $\gamma_{cm}\sqrt{s}$ and $\beta_{cm}\,\gamma_{cm}\sqrt{s}$, where β_{cm} and γ_{cm} are, respectively the velocity and Lorentz factor of the CMS in the LS. Therefore the rapidity of the CMS in the LS is

$$y_{cm} = \frac{1}{2}\,\ln\left[\frac{\gamma_{cm}\sqrt{s} + \beta_{cm}\,\gamma_{cm}\sqrt{s}}{\gamma_{cm}\sqrt{s} - \beta_{cm}\,\gamma_{cm}\sqrt{s}}\right] = \frac{1}{2}\,\ln\left[\frac{1+\beta_{cm}}{1-\beta_{cm}}\right] \tag{1.9}$$

The rapidity of a particle is actually the relativistic realization of the velocity, and in one Lorentz frame it is related to the rapidity in the other by an additive constant. As for example the rapidity of a particle (y) in LS is related to the same (y^*) in CMS by the simple relation $y = y^* + y_{cm}$. Let us denote the projectile by P and the target by T. In a fixed target experiment $p_{_T} = 0$, $E = m_{_P}\cosh y_{_P}$ and $p_{_L} = m_{_P}\sinh y_{_P}$ for the incident particle, where $m_{_P}$ is its rest mass and $y_{_P}$ the rapidity. Therefore,

$$y_{_P} = \cosh^{-1}\left(\frac{E}{m_{_P}}\right) = \cosh^{-1}\left(\frac{\sqrt{s}_{NN}}{2m_N}\right) \qquad \text{or} \qquad y_{_P} = \sinh^{-1}\left(\frac{p_{_L}}{m_{_P}}\right)$$

• **Pseudorapidity Variable:** In some experiments variables like E, $\boldsymbol{p}$ or the rest mass of a particle may not be easily measured. In such cases it is convenient to use the *pseudorapidity* (η) variable to characterize the particle which requires only the measurement of the emission angle (θ) with respect to the beam direction. The η variable is defined as,

$$\eta = -\ln\left[\tan\left(\theta/2\right)\right] \tag{1.10}$$

At high-energy ($|\boldsymbol{p}| \gg m$) the pseudorapidity can also be approximated to the rapidity,

$$\eta = \frac{1}{2}\ln\left(\frac{|\boldsymbol{p}| + p_{_L}}{|\boldsymbol{p}| - p_{_L}}\right) \approx y \tag{1.11}$$

Using Eq. (1.8) and Eq. (1.10) y and η can be expressed in terms of each other

$$y = \frac{1}{2}\ln\left[\frac{\sqrt{p_{\perp}^2\cosh^2\eta + m^2} + p_{\perp}\sinh\eta}{\sqrt{p_{\perp}^2\cosh^2\eta + m^2} - p_{\perp}\sinh\eta}\right]; \eta = \frac{1}{2}\ln\left[\frac{\sqrt{m_{\perp}^2\cosh^2 y + m^2} + m_{\perp}\sinh y}{\sqrt{m_{\perp}^2\cosh^2 y + m^2} - m_{\perp}\sinh y}\right].$$

The distribution of the number of detected particles (N) in terms of $p_{_\perp}$ and y can therefore, be related to the distribution in terms of $p_{_\perp}$ and η as,

$$\frac{d^2N}{d\eta\, d\boldsymbol{p}_{_\perp}} = \left(1 - \frac{m^2}{m_{\perp}^2\cosh^2 y}\right)^{\frac{1}{2}} \frac{d^2N}{dy\, d\boldsymbol{p}_{_\perp}} \tag{1.12}$$

The differential d^3p/E is a Lorentz invariant quantity. One can express it as,

$$d^3p/E = d\boldsymbol{p}_{_\perp}\, dy = p_{_\perp}\, dp_{_\perp}\, d\varphi\, dy = m_{_\perp}\, dm_{_\perp}\, d\varphi\, dy. \tag{1.13}$$

The Lorentz invariant differential cross-section $E\, d^3\sigma/dp^3 \equiv E\, d^3N/dp^3$, also called the invariant yield, can now be expressed in terms of measurable quantities as,

$$E\frac{d^3\sigma}{dp^3} \propto \frac{1}{m_{_\perp}}\frac{d^3N}{dm_{_\perp}\, d\varphi\, dy} = \frac{1}{2\pi\, m_{_\perp}}\frac{d^2N}{dm_{_\perp}\, dy} = \frac{1}{2\pi\, p_{_\perp}}\frac{d^2N}{dp_{_\perp}\, dy}. \tag{1.14}$$

1.3 Nucleus-Nucleus Collision at High-energy

A high-energy AB collision is a highly complex dynamical event. The control parameters are the collision energy and the size of the colliding system. We expect that for the short-range hadronic interactions the collision geometry should determine the amount of matter participating in nuclear collisions. The collision geometry is a very important and therefore should be very carefully explored. The early age experimental results confirm the role of this simple geometric picture of nuclear collision dynamics. The reaction radius, defined as

the square root of the reaction cross section (σ), increases linearly with the geometric size of the colliding system described by the sum of their radii as [14],

$$\sigma^{1/2} \propto \left[A^{1/3} + B^{1/3}\right]. \tag{1.15}$$

This result confirms that for local deposition of energy and baryon number to take place the colliding nuclei need to 'touch' each other. At high energies in the laboratory system ($E_{\rm lab} \sim$ a few GeV per nucleon) in the center of momentum frame, due to Lorentz boost both the colliding nuclei look like two discs, contracted along the direction of the boost with transverse radii respectively, say R_A and R_B, approaching each other. Figure 1.3 shows a schematic

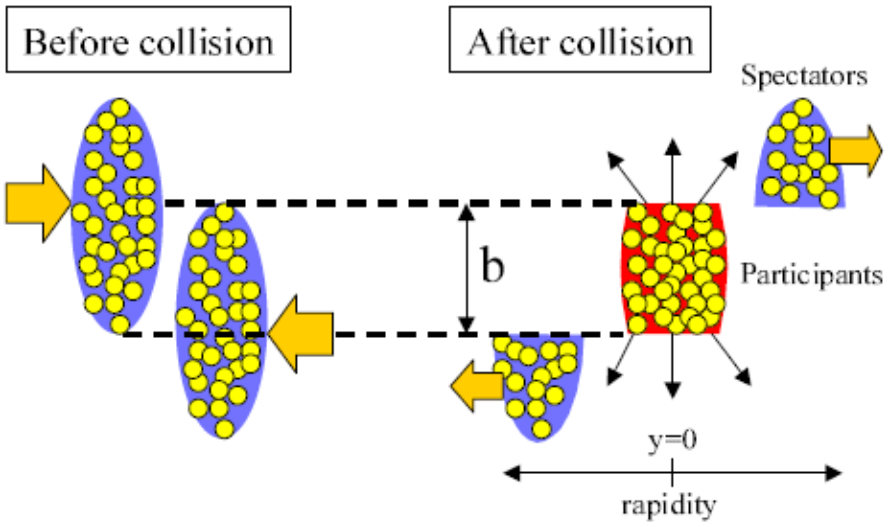

Figure 1.3: Geometry of a nucleus-nucleus collision.

drawing of such an interacting system. Nucleons that directly participate in the collision are called the 'participants', and the rest that do not participate are called the 'spectators'. The number of participating nucleons (N_{part}) should in principle be geometrically determined from the impact parameter (b) of the collision, that in principle can vary between 0 and $R_A + R_B$. Collisions close to the $b \approx 0$ side are called central events, while those on the $b \approx R_A + R_B$ side are called peripheral events, and the entire set of events with $0 \leqslant b \leqslant R_A + R_B$ is called a minimum bias sample. However, b cannot be directly measured in an experiment. Generally, any observable that varies monotonically with b can be used to represent the impact parameter. The average charged particle multiplicity N_{ch}, the transverse energy ($E_{\perp}$) and the missing forward energy are suitable for this purpose. For most central collisions the missing forward energy approaches zero, thereby posing extra difficulty to use it as a trigger condition. Therefore, two assumptions are made: (i) on an average $E_{\perp}$ released in a collision is proportional to N_{part}, and (ii) N_{ch} per collision is proportional to N_{part}. Now the minimum bias $E_{\perp}$ or N_{ch} distribution can be used to

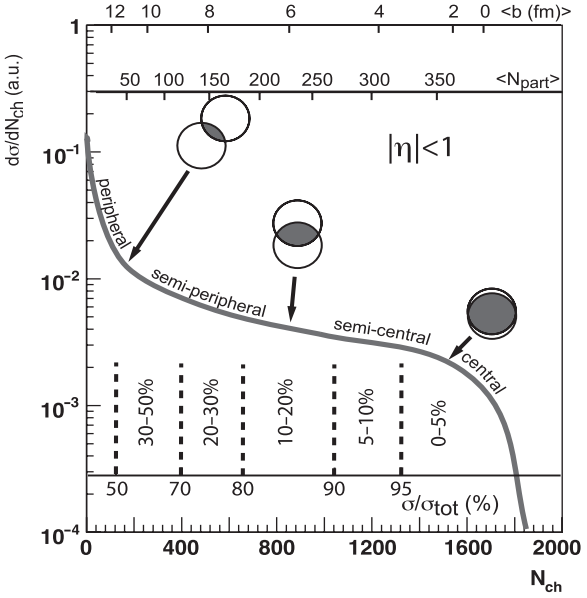

Figure 1.4: Multiplicity distribution as a tool to determine centrality of AB collision.

determine the average centrality of a sub-sample of events, while the energy carried in the extreme forward direction can be used to determine the number of spectator nucleons. As for example, events with the highest 5% value of N_{ch} should correspond to the 5% most central collisions. The correlation between centrality and the impact parameter can be established by Galuber-type Monte Carlo simulations and by employing Woods-Saxon type nuclear density profile [15]. The Glauber model treats the AB collision as a superposition of many NN collisions, assumes that at high-energies nucleons travel in straight lines (eikonal approximation), an inelastic NN collision takes place if two nucleons come within a distance $d \leqslant \sqrt{\sigma_{NN}^{inel}/\pi}$, and after each such collision if a hadron is excited, it will subsequently interact with other hadrons with the same cross-section as the original nucleons, σ_{NN}^{inel} being the NN inelastic scattering cross section. According to this model in hard processes, where large momentum transfer takes place, N_{part} proportionally varies with A, whereas the number of NN binary collisions N_{coll} grows as $A^{4/3}$. The correlation between N_{ch}, centrality and N_{part} is schematically shown Fig. 1.4 [15].

Each incoming nucleus can be looked upon as a coherent cloud of partons, more precisely as color-glass-condensates where the nucleons possess only longitudinal momentum/energy. The nucleons undergo successive collisions, as a result of which new (transverse) degrees of freedom are excited, and a significant fraction of the incoming kinetic energy is deposited in the central region leading to the formation of a high-energy, high-density fireball, a highly non-equilibrium state. This is still coherent and liberation of partons from this state takes a finite amount of proper time ($<$ fm/c). Subsequent collisions among partons lead to a nearly thermalized (local thermalization) state. This happens at a time of the order of 1 fm/c, a less

understood aspect of the entire process. When the incident energy involved is extremely high ($\sqrt{s} \geqslant 200$A GeV) and the participating nucleons are far apart in phase space, the colliding nuclei cannot stop each other and are said to be 'transparent' with respect to each other. As mentioned above, still significant amount of energy will be deposited in the central reaction zone which is gradually converted into formation of $q\overline{q}$ pairs. A large number of final state particles will be produced in the form of mesons, while the relative abundance of net baryon content of the state will be small. Models based on hydrodynamics are used for theoretical understanding of such states. Once again this may eventually lead to QGP formation at high temperature and small chemical potential, a state that perhaps has already been created in BNL Relativistic Heavy-ion Collider (RHIC) and in CERN Large Hadron Collider (LHC) experiments. Subsequent evolution of the system proceeds following a relativistic imperfect fluid dynamics.

On the other hand, if the nucleons stemming out of the projectile and target nuclei can significantly stop each other, we expect a baryon rich state to develop in the central reaction zone that may ultimately lead to a baryon rich QGP. Nuclear stopping is a measure of the efficiency of converting the incoming longitudinal energy into transverse degrees of freedom and slowing down of the incoming nucleus (nuclei). Using the Alternating Gradient Synchrotron (AGS) at Brookhaven National Laboratory (BNL) and Super-proton Synchrotron (SPS) at Center for Nuclear Research (CERN), in experiments up to 60A GeV collision energy involving ^{28}Si or ^{32}S projectiles almost complete stopping has been observed. Significant redistribution of the total initial baryon number carried by the interacting nucleons takes place, leading to a high baryo-chemical potential of the equilibrated state. The underlying physics issues are addressed through non-perturbative QCD and/or through hadronic transport models. In a symmetric collision ($A_{_P} = A_{_T}$), if a complete overlap between projectile and target is reached then the stopping is large, and such collisions are best for studying a free expansion of hot and dense nuclear matter in vacuum. Stopping is typically measured by the average rapidity loss defined as,

$$\langle \delta y \rangle = y_{_P} - \langle y_b \rangle = y_{_P} - \frac{2}{N_{part}} \int_0^{y_{_P}} y \, \frac{dN_{_{b-\bar{b}}}}{dy} \, dy, \tag{1.16}$$

where $\langle y_b \rangle$ is the net average baryon rapidity after the collision. The average scaled rapidity shift $\langle \delta y / y_{_P} \rangle \approx 0.27$ does not significantly change up to SPS energy ($E_{\rm lab} = 200$A GeV) [16], which signifies that for comparable system sizes the normalized rapidity densities do not change with beam energy. Corresponding energy loss (ΔE) can also be estimated,

$$\Delta E = \int_{-y_{_P}}^{y_{_P}} \langle m_{_\perp}(y) \rangle \, \frac{dN_{_{b-\bar{b}}}}{dy} \, \cosh y \, dy, \tag{1.17}$$

which comes out to be $\Delta E = 25.7 \pm 2.1$ TeV at the top RHIC energy [17]. It should also be noted that an incomplete stopping and a longitudinally expanding source lead to similar rapidity distributions, an issue that should be properly taken care of.

The energy content available for particle production in an AB collision is the basic and most important quantity. This will depend globally on $\sqrt{s}_{_{NN}}$ and collision centrality, and locally on $p_{_\perp}$ and y. The $p_{_\perp}$ spectra of produced particles can in general be divided into a low-$p_{_\perp}$ and a high-$p_{_\perp}$ part. The low-$p_{_\perp}$ part due to the random kinetic and collective motion of particles present in the fireball, has a thermal origin and can be described by an exponentially decaying function. The high-$p_{_\perp}$ part on the other hand is dominated by hard scatterings and requires a power-law. The inverse slope of the $p_{_\perp}$ spectrum is the 'effective temperature' (T_e) of the source (here the fireball) from which the particles are originating. T_e can be measured from the knowledge of $\langle p_{_\perp} \rangle$ defined as,

$$\langle p_{_\perp} \rangle = \frac{\int_0^\infty p_{_\perp} \left(\frac{dN}{dp_{_\perp}}\right) dp_{_\perp}}{\int_0^\infty \left(\frac{dN}{dp_{_\perp}}\right) dp_{_\perp}} = \frac{\int_0^\infty {p_{_\perp}}^2 f(p_{_\perp})\, dp_{_\perp}}{\int_0^\infty p_{_\perp} f(p_{_\perp})\, dp_{_\perp}}. \tag{1.18}$$

Here $f(p_{_\perp})$ is the $p_{_\perp}$ distribution function that can be approximated by an exponential function as,

$$f(p_{_\perp}) = \frac{dN}{d\boldsymbol{p}_{_\perp}} = \frac{1}{2\pi}\left(\frac{dN}{p_{_\perp} dp_{_\perp}}\right) \propto \exp(-m_{_\perp}/T_e). \tag{1.19}$$

One can use the above form of $f(p_{_\perp})$ to determine the average value of say $m_{_\perp}$:

$$\langle m_{_\perp} \rangle = \frac{\int_0^\infty p_{_\perp}\, m_{_\perp}\, \exp(-m_{_\perp}/T_e)\, dp_{_\perp}}{\int_0^\infty p_{_\perp}\, \exp(-m_{_\perp}/T_e)\, dp_{_\perp}} = \frac{2T_e^2 + 2mT_e + m^2}{m + T_e}. \tag{1.20}$$

For $\langle p_{_\perp} \rangle \gg$ the rest mass m of the particle under consideration, $\langle m_{_\perp} \rangle \approx \langle p_{_\perp} \rangle \approx 2T_e$. Integrating the invariant yield over the entire $p_{_\perp}$ region one gets the rapidity distribution dN/dy of produced particles. Significant amount of information on AB collisions can be extracted by studying the rapidity distribution. Particle identification is necessary for the purpose, which may not be possible in all experiments. Under such circumstances the pseudorapidity distributions are used. At very high-energies dN/dy should exhibit a plateau which due to the transformation given in Eq. (1.12) gets depleted by a small extent around $\eta^* = \eta - \eta_{cm} = 0$. In the CMS the depletion factor is $(1 - m^2/ < m_{_\perp}^2 >)^{1/2}$, whereas in the LS the peak of the distribution is located around half of the beam rapidity $y_{_P}/2$, and the depletion factor is $[1 - m^2/\left\{< m_{_\perp}^2 > \cosh^2(y_{_P}/2)\right\}]^{1/2}$. Due to additive nature of the rapidity variable its distribution remains unchanged as one moves from the LS to the CMS or vice versa. In any relativistic AB collision usually there is a central particle producing region which results from the nucleons directly participating in the collision, and two baryon rich fragmentation regions (target and projectile) that contain the spectator

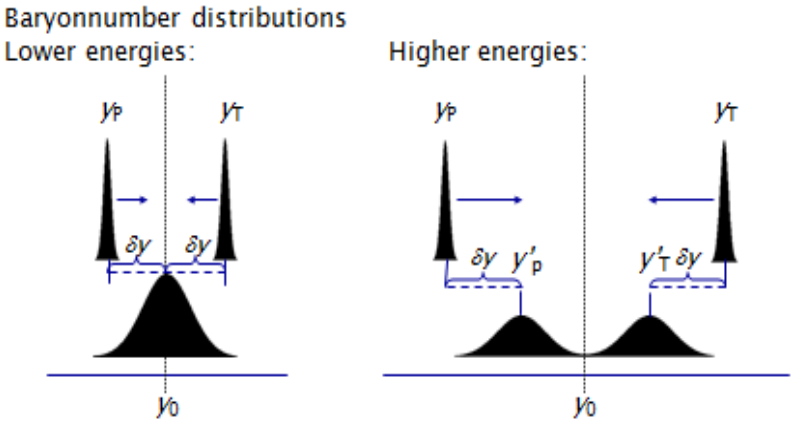

Figure 1.5: Stopping in nucleus-nucleus collisions.

nucleons. When the colliding nuclei are 'transparent' with respect to each other, they leave a trail of energy in the form of stretched out strings in between projectile and target rapidities. The strings subsequently fragment and the central region is populated (mostly) by different types of mesons. The baryons (nucleons) continue to move out of the central rapidity region apart from a down-shift in their rapidity values necessary for conservation of energy. On the other hand when the colliding nuclei substantially stop each other, the central rapidity region is filled up with both energy and baryons. Under the most extreme circumstances of complete stopping, the projectile and target baryons loose all memory of their initial states. Correspondingly, the difference (if there is any) between the energy and baryon number distributions in longitudinal and transverse directions with respect to the collision axis will be very little. These two extreme situations are schematically represented in Fig. 1.5 We understand that the rapidity gap $\Delta y = y_P - y_T$ i.e., the difference between the rapidity values of projectile and target, is important for characterizing the central region. For targets fixed in the LS $y_T = 0$ and $\Delta y = y_P$. Accordingly $\cosh \Delta y = E_P/m_P$. In collider experiments involving a head on symmetric colliding system, the CMS is at rest in LS and $\Delta y/2$ is the rapidity of projectile/target. With increasing $\sqrt{s}_{NN}$ rapidity gap is found to increase as, $\Delta y \propto \ln \sqrt{s}$ [18], thereby enabling us to study the central region without having actually to account for particles spilling over from the fragmentation regions. Up to SPS energy the rapidity distribution do not show any plateau and can in stead be described by a single Gaussian having a width $\sigma(y)$ nearly proportional to Δy $(= 2 - 3)$ rapidity units. Any system having a preferentially longitudinal expansion of the particle emitting source will therefore, have to have a reasonably large rapidity gap $(\Delta y > 3)$ which occurs beyond the SPS energy. Experimental data suggest that nuclear/partonic stopping is present in the primordial, first generation collisions at the microscopic level. Rapidity distributions of particle multiplicity and/or transverse energy exhibit qualitatively similar shapes, which also evolve similarly with $\sqrt{s}$ in pp, $p\bar{p}$ and e^+e^- reactions on one hand, and in central AB collisions on the other. One can formulate a nuclear modification factor for the bulk hadron

rapidity distributions as,

$$R_{_{AA}} = \frac{dN_{ch}/dy \text{ in } AA}{0.5\, N_{part}\; dN_{ch}/dy \text{ in } pp}, \tag{1.21}$$

where N_{part} is the average number of participating nucleons, and for AA collisions $0.5\, N_{part}$ is the average number of opposing nucleon pairs. If the contribution to the total yield from each such opposing pairs is same as that from pp collision at same $\sqrt{s}$, then $R_{_{AA}} = 1$. However, in RHIC and LHC experiments $R_{_{AA}}$ is found to be more than unity, thereby indicating higher stopping in nuclear collisions.

1.3.1 Space-time Evolution of AB Collision

In the CMS of a two-body collision the interacting nuclei follow trajectories very close to the light cone because their velocities are very close to that of the light [18]. We consider both longitudinal space co-ordinate (z) and the time (t) to be zero at the collision point. After the collision a large amount of the energy/matter density or both are deposited in the reaction zone around $z \sim 0$ [19]. If the energy/matter density is so large that the temperature/chemical potential of the created state exceeds the respective critical values required for a phase transition, one may achieve a state of deconfined quarks and gluons. Rescattering among the partons may then lead to thermalization and chemical equilibration. Subsequent expansion and cooling down of the medium will be governed by the equation of this deconfined state. As the system expands and cools down hadronization takes place. Assuming that an equilibrated color conducting deconfined state is created and based on some general arguments it is possible to roughly divide the entire sequence of evolution of a high-energy AB collision into several stages as illustrated in Fig. 1.6.

(i) The initial collisions among the projectile and target nucleons take place during the passage time of the colliding nuclei, which is $\sim 2R/\gamma_{CM}$ for a symmetric and $\sim (R_A + R_B)/\gamma_{CM}$ for an asymmetric collision. Here R, R_A and R_B are the respective nuclear radii, and γ_{CM} is the Lorentz factor of the CMS in the LS. During this stage intense matter compression and heating take place. Due to inelastic processes initial longitudinal energy is converted to new internal and transverse degrees of freedom with breaking up of initial baryon structures. This initial stage of collision is labeled as a 'pre-equilibrium'. Processes like parton-parton hard scattering predominantly take place in the overlap region of two colliding nuclei, depositing thereby a large amount of energy in the central ($z \sim 0$) region. The characteristic time of the pre-equilibration state is same as the passage time.

(ii) After the short pre-equilibration time a 'fireball' is created, where depending on the initial conditions thermal and chemical equilibrium may be established. If a QGP like

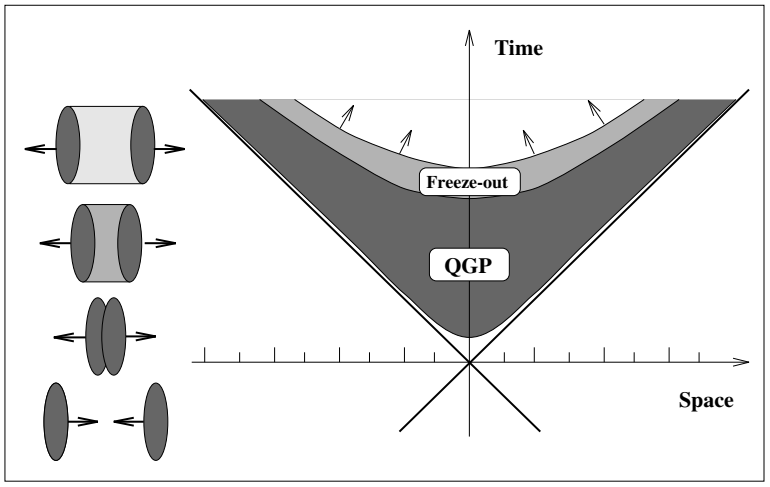

Figure 1.6: Schematic of spacetime evolution of a high energy nucleus-nucleus collision in the center-of-mass frame of two colliding nuclei.

state is formed it will be dominated by parton-parton and/or string-string scattering and the energy density is expected to reach a high value. The transition from a hadron gas to the QGP may occur at or around the Hagedron limit of temperature $T \approx 170$ MeV [7]. The precise value of the transition temperature (T_c) and how high the temperature must rise before the plasma can be considered as weakly coupled, can only be determined by an accurate and nonperturbative simulation of the QCD equation of state. Subsequently the volume of the QGP state rapidly expands and the energy density, temperature and/or baryon density of the fireball decrease. The high energetic quarks and gluons may also produce 'jets' which propagate through the medium so created.

(iii) If a first-order phase transition is assumed, a 'mixed phase' is expected to exist between the QGP and the hadronic state, in which quarks and gluons are again confined into hadrons at a critical point. At the mixed phase the entropy density is transferred to lower degrees of freedom and therefore, the system is prevented from a fast expansion and cooling due to the 'softest point' defined by a minimum value of energy density/-pressure (ε/p) in the equation of state. This leads to a maximum in the lifetime of the mixed phase, which is expected to last for a relatively long time ($\tau > 10$ fm/c) during the softening of the equation of state.

(iv) The expanding fireball first reaches a chemical freeze-out stage when the inelastic interaction between the partons cease to take place and the relative abundance of every single particle species does no more change. The partons gradually start to recombine and produce different varieties of color neutral particles. In the hadronic phase the system maintains a collective expansion via hadron-hadron elastic interactions, thereby decreasing the temperature of the fireball. As the elastic collisions between

the particles slow down, the expanding system reaches a stage of kinetic freeze-out, and the final state particles freely stream out from the medium.

1.3.2 Experimental Scenario

The experimental studies on high-energy AB interaction has been carried out over about the last four decades. In the early days of high-energy heavy-ion and not so heavy-ion physics, the experimental scenario was dominated by some fixed target programmes like, (i) the Bevatron at Lawrence Berkeley National Laboratory (LBNL), (ii) the Synchrophasotron at Joint Institute of Nuclear Research (JINR), (iii) the Alternating Gradient Synchrotron (AGS) at Brookhaven National Laboratory (BNL) and (iv) the Super Proton Synchrotron (SPS) at CERN. Despite some experimental results suggesting early signal(s) of QGP formation [20], a clear signal in this regard was not confirmed in these fixed target experiments.

Table 1.1: Accelerator facilities in relativistic heavy-ion physics.

Accelerator	Start Year	Max. Energy	Projectiles	Experiment type
Bevalac Berkeley	1984	$<$ 2A GeV	^{12}C, ^{40}Ca, ^{84}Kr, ^{238}U	Fixed target
Synchrophasotron JINR, Dubna	1975	4.5A GeV	^{12}C, ^{24}Mg, ^{20}Ne, ^{28}Si	Fixed target
BNL-AGS Brookhaven	1986	14.6A GeV	^{28}Si	Fixed target
BNL-AGS Brookhaven	1992	11A GeV	^{197}Au	Fixed target
CERN-SPS Geneva	1986	200A GeV	^{16}O, ^{32}S	Fixed target
CERN-SPS Geneva	1994	200A GeV	^{208}Pb	Fixed target
GSI-SIS Darmstadt	2002	2A GeV	^{84}Kr, ^{197}Au	Fixed target
BNL-RHIC Brookhaven	2002	$\sqrt{s}_{NN} = 200$ GeV	^{39}Cu, ^{197}Au	Collider
CERN-LHC Geneva	2008	$\sqrt{s}_{NN} = 5.5$ TeV	^{16}O, Ar, Pb	Collider
GSI-SIS300 Darmstadt	2017	45A GeV	^{59}Ni, ^{197}Au	Fixed target
NICA JINR, Dubna	2017	$\sqrt{s}_{NN} \sim 5$A GeV	^{197}Au, ^{238}U	Collider

At the beginning of 21st century the experimental study of high-energy nuclear collisions entered into a new era with the Relativistic Heavy-Ion Collider (RHIC) started functioning at BNL. This was followed by the establishment of Large Hadron Collider (LHC) at CERN, making provision for collision energies higher than RHIC more than by an order. For the first time in any terrestrial laboratory, the experiments at RHIC and LHC started to confirm the creation of a color deconfined extended QCD state like the QGP at high temperature and low chemical potential. The analysis, refinement of accumulated data, and physics analysis are still going on. To complement the RHIC and LHC experiments and to study the QCD state of high baryo-chemical potential, the Compressed Baryonic Matter (CBM) experiment is being designed at the Facility for Anti-proton and Ion Research (FAIR) at GSI, Darmstadt, which is expected to be commissioned some time in 2017-'18 [21]. The major heavy-ion programmes undertaken till date are summarized in Table 1.1. Some of the major experimental facilities and their importance in high-energy heavy-ion research are summarily outlined within the limited scope of this thesis.

1.3.3 Experiment at the BNL-AGS

Since 1960, the Alternating Gradient Synchrotron (AGS) has been one of the world's premier particle accelerator facility. The AGS receives proton beam of energy 200 MeV from the linear accelerator (LINAC) of Brookhaven and accelerates it up to energy 33 GeV. The AGS Booster, constructed in 1991, further augments the capability of the AGS, enabling it to accelerate more intense proton beams as well as heavy-ions such to higher energies. Currently the AGS is being used as an injector for the RHIC. Some features of major experiments performed in the BNL-AGS like their major detector component(s) and observable(s), are given in Table 1.2. However, a large number of small experiments were also carried out at the BNL-AGS facility, and the present thesis is based mainly on the data collected from one such experiment (E847).

1.3.4 Experiment at the CERN-SPS

The Super Proton Synchrotron (SPS) was the second largest of CERN accelerators, and now it is embedded with the Large Hadron Collider (LHC). The SPS had about 7 KM circumference with 1317 conventional electromagnets including 744 dipoles to bend the beams round the ring. A proton beam of 400 GeV energy was first extracted from the SPS in 1976 with a flux of 5×10^{12} particles per pulse. Latter SPS was modified to accelerate heavy-ions. The ions partially stripped of their electrons originate from an electron cyclotron resonance, pass through a radio frequency quadrapole, and injected into a LINAC, where

Table 1.2: Four experiments at BNL-AGS: its major detector components and the important observations.

Experiment	Major detector(s)	Observation(s)
E787	Photomultiplier tube (PMT) Drift chamber YAlO light pulser	rare decay, specially $K^+ \to \pi^+ \nu\bar{\nu}$
E802	Zero-degree calorimeter (ZDC) Pb-glass calorimeter (PBGL) Target multiplicity array (TMA) Magnetic spectrometer	E_{ZD}, ρ, η $p, \bar{p}, d, \pi^{\pm}$ $K^{\pm}$ spectrum
E810	Time projection chamber (TPC)	Momenta and angles of charged particles
E814	NaI+U calorimeter Target calorimeter (TCAL) Silicon multiplicity counter Participant calorimeter Forward spectrometer	Transverse energy $E_{\perp}$, multiplicity in the forward direction

they are accelerated to an energy of 4.2 MeV. To get rid of the remaining electrons the ions are then allowed to pass through a stripper foil, and then successively accelerated by the proton synchrotron booster and proton synchrotron. The ions come out of the proton synchrotron with an energy of 4.2A GeV, and then pass through another stripper, that completely ionizes them. They are then injected into the SPS and accelerated to the highest possible energies. The ions are extracted at seven different points. Many experiments were performed in the CERN-SPS over a period of almost 22 years. The experiments may be divided into two categories, the 'Oxygen-Sulfur' age and the 'Lead' age experiments. Short summary of some of the major heavy-ion experiments at CERN-SPS are given in Table 1.3 and Table 1.4 [22]. Like in the BNL-AGS case, many small experiments were performed using the SPS facility too.

1.3.5 Experiment at the BNL-RHIC

The Relativistic Heavy Ion Collider (RHIC) at Brookhaven National Laboratory is one of only two major collider facilities in the world, the other being the CERN-LHC. Also RHIC is the world's first and only polarized proton collider. RHIC is composed of two independent rings of circumference 3.8 km. containing a total of 1740 superconducting magnets. In principle RHIC can collide any species of nucleon with any other. Since its inception the collider has so far operated at 15 different $\sqrt{s}_{NN}$ values at six different species combinations. The startup of the RHIC in the year 2000 provided a major advancement leading to the discovery of the QGP, which was announced in 2005. The results [23, 24] indicated that

Table 1.3: The Oxygen-Sulfur age 'large' experiments at CERN-SPS: its major detector component(s) and the important observation(s).

Experiment	Major detector(s)	Observation(s)
NA34	U-calorimeter Liquid Ar-calorimeter Si-pad detectors External spectrometer	 $E_\perp$, $\rho(\eta)$, π^-, γ Low mass muon pairs
NA34	Zero degree calorimeter (ZDC) Right calorimeter Photon position detector Streamer chamber Vertex magnet	 E_{ZD}, $E_\perp$, $\rho(\eta)$, π^-, p, γ, K^0_s, Λ, $\bar{\Lambda}$
NA36	Time projection chamber	K^0_s, Λ, $\bar{\Lambda}$, Ξ, Ω
NA38	Electromagnetic calorimeter Di-muon spectrometer	$E_\perp$, J/ψ, muon pair
WA80	ZDC, mid-rapidity calorimeter Mid-rapidity multiplicity detector Large angle multiplicity detector Pb-glass photon detector	 E_{ZD}, $E_\perp$, $n_{\rm ch}$ $\rho(\eta)$, γ, π^0
NA85	Ω-spectrometer, MWPC	K^+, K^0, Λ, $\bar{\Lambda}$, $\Xi^\pm$

Table 1.4: The Lead age experiments at CERN-SPS: its major detector component(s) and the important observation(s).

Experiment	Major detector(s)	Particles	y(lab)
NA44	Focusing spectrometer Time of flight (TOF)	K^+	2.5 – 3.5
NA49	Time projection chamber	K^+, K^0, ϕ Λ, $\bar{\Lambda}$, $\Xi^\pm$	3.0 – 5.0
NA50	Dimuon spectrometer	ϕ	3.0 – 4.0
NA52	Beam spectrometer	K^+	1.4 – 6.0
WA97	Silicon Telescope	$K^+, K^0, \Lambda, \bar{\Lambda}$ $\Xi^\pm, \Omega^\pm$	2.4 – 3.4

instead of behaving like a 'gas' of free quarks and gluons, the partonic matter created in RHIC at $\sqrt{s}_{NN} = 200$ GeV behaves more like an 'imperfect fluid'. The matter is much more strongly interacting than what was originally expected and possesses a non-zero viscosity [12, 17, 25, 26], which inspired to give it the new name 'sQGP' (strongly interacting QGP) [27]. The properties are quite different from the properties of the state of matter created

in CERN-SPS, which also claimed of a 'new state of matter' [28]. However, the results in the past two years from Pb + Pb measurements at the CERN-LHC at $\sqrt{s}_{NN} = 2.76$ TeV confirm the RHIC discoveries [23, 24], and add some new information too. Four major collaborative experiments have so far been performed at RHIC. Very brief description of them are given below.

• **The BRAHMS Experiment:** The BRAHMS (Broad Range Hadron Magnetic Spectrometer) setup was one of the smaller detectors of the RHIC. The BRAHMS experiment was designed to measure charged hadrons over a wide range of rapidity and transverse momentum to study the reaction mechanisms of the relativistic heavy-ion interactions and the properties of a highly excited nuclear matter formed in these reactions. The experiment took its first data in the year 2000 and completed data-taking in 2006.

• **The PHOBOS Experiment:** The PHOBOS detector was designed to examine and analyze a very large number of Au ion collisions. For each collision, the detector gives a global picture of the consequences of collision and information about a small subset of the nuclear fragments ejected from the high-energy density region. PHOBOS consisted of many silicon pad detectors surrounding the interaction region. With these detectors it was possible to count the total number of produced particles and study their angular distribution. With this array PHOBOS looked for unusual features, like fluctuations in the number of particles or in their angular distributions. Fluctuations of global/local variables in an event can be a characteristic of phase transition. In order to obtain more detailed information about these events, the PHOBOS detector also has two high-quality magnetic spectrometers, which study 1% of the produced particles in detail. The PHOBOS experiment was able to measure quantities like temperature, size and density of the fireball produced in the collision. It also studied the ratios of various particles produced.

• **The STAR Experiment:** The Solenoidal Tracker at RHIC (STAR) is a detector which specializes in tracking the thousands of particles produced in each collision at RHIC. Unlike other physics experiments where a theoretical idea can be tested directly by a single measurement, STAR makes use of a variety of simultaneous studies in order to draw strong conclusions about the QGP. This is due both to the complexity of the system formed in the high-energy nuclear collision and the unexplored landscape of the physics we study. The STAR detector therefore consists of several types of detectors, each specializing in detecting certain types of particles or characterizing their motion. These detectors work together with an advanced data acquisition and subsequent physics analysis that allows final statements to be made about the collision.

• **The PHENIX Experiment:** The Pioneering High Energy Nuclear Interaction Experiments (PHENIX) is the largest of the four experiments that have taken data at the

RHIC. PHENIX is an exploratory experiment for the investigation of high-energy collisions of heavy-ions and protons. PHENIX is designed specifically to measure direct probes of the AB collisions such as electrons, muons, and photons. The primary goal of PHENIX is to discover and study the QGP. The PHENIX set-up consists of a collection of detectors, each of which performs a specific role in the measurement. The detectors are grouped into two central arms, which are capable of measuring a variety of particles including pions, protons, kaons, deuterons, photons, and electrons, and two muon arms which focus on the measurement of muon particles. There are also additional event characterization detectors that provide additional information about a collision, and a set of three huge magnets that bend the trajectories of the charged particles.

1.3.6 Experiment at the CERN-LHC

The Large Hadron Collider (LHC), the world's largest and most powerful particle accelerator, is the latest addition to CERN's accelerator complex. It consists of a 27 km. long ring of superconducting magnets with a number of accelerating structures to boost the energy of the particles along their path. In the LHC heavy-ion programs, beams of nuclei collide at 30 times higher energies than in RHIC. The objective is to produce nuclear matter at the highest temperatures and densities ever studied in the laboratory, and to investigate its properties in detail. This LHC facility is expected to lead to basic new insights into the nature of the strong interaction between fundamental particles. In the LHC heavy-ion programme three experiments, ALICE, ATLAS and CMS, aim to produce and study this extreme high temperature state of matter and provide novel access to the question of how most of the mass of visible matter in the universe was generated during the first microseconds after the Big-Bang. The ALICE along with LHCb have specialized detectors for analyzing the LHC collisions in relation to specific phenomena. Two further experiments, TOTEM and LHCf, are much smaller in size. They are designed to focus on 'forward particles' (protons or heavy-ions). These are particles that just brush past each other as the beams collide, rather than meeting head-on. Brief summary of the three major heavy-ion experiments at the LHC are given below.

• **The ATLAS Experiment:** ATLAS, being a general purpose detector system, investigates a wide range of physics, including the search for the Higgs boson, extra dimensions, and particles that could make up dark matter. ATLAS has recorded many sets of measurements on the particles created in collisions - their paths, energies, and identities. This is accomplished in ATLAS through six different detecting sub-systems that identify particles and measure their momentum and energy. Another vital element of ATLAS is the huge magnet system that bends the paths of charged particles for momentum measurement.

The interactions in the ATLAS detectors create an enormous data flow. To analyze these data, ATLAS developed a very advanced trigger and data acquisition system and a large computing system.

• **The ALICE Experiment:** The ALICE (A Large Ion Collider Experiment) experiment at LHC is designed to study the collisions of heaviest stable ions (Pb). ALICE studies the physics of strongly interacting matter at extreme energy densities, where the formation of the QGP is expected. For this purpose, ALICE carries out a comprehensive study of the hadrons, electrons, muons and photons produced in Pb + Pb collisions. ALICE is also studying proton-proton (*pp*) collisions both for the purpose of comparison with Pb + Pb collisions and for physics analysis where ALICE is competitive with other LHC experiments. At the beginning of 2013 just before the LHC shutdown, the ALICE experiment got another opportunity to collect exciting data with the asymmetric p + Pb collisions. These data are crucial for understanding the complexity of the Pb + Pb interaction in many levels and are a necessary supplement for the baseline of *pp* data. In fact, the data from the p + Pb collisions will represent an ultimate benchmark for the already published results from Pb + Pb collisions. It will definitely allow to decouple the cold nuclear matter effects and thus will shed light to our quest for the QGP.

• **The CMS Experiment:** The Compact Muon Solenoid (CMS) experiment also uses a general purpose detector to investigate a wide range of physics, including the search for Higgs boson, extra dimensions, and particles that could make up dark matter. Although it has the same scientific goals as the ATLAS experiment, it uses different technical solutions and design of its detector magnet system to achieve these. The CMS detector is built around a huge solenoid magnet. This takes the form of a cylindrical coil of superconducting cable that generates a magnetic field of about 4 T. The magnetic field is confined by a steel 'yoke' that forms the bulk of the detector's weight of 12500 tones. An unusual feature of the CMS detector is that, instead of being built in-situ underground like the other giant detectors of the LHC experiments, it was constructed on the surface, before being lowered underground in 15 sections and reassembled.

1.3.7 The FAIR-CBM Experiment

The Compressed Baryonic Matter (CBM) experiment will be one of the major scientific programs in the future Facility for Antiproton and Ion Research (FAIR) in GSI, Darmstadt. Laid out as a fixed-target experiment, the CBM research program will explore the QCD phase diagram in the region of high baryon densities using proton-nucleus and AB collisions at beam energies between 10A to 45A GeV. This includes finding out an appropriate equation of state for the nuclear matter at high densities, search for the deconfinement, detailed study

of the QCD phase diagram and chiral phase transitions [21]. The CBM detector will be so designed as to measure both bulk observables with large acceptance and rare diagnostic probes like charmed particles and vector mesons decaying into lepton pairs. Hadronic, leptonic and photonic observables will be measured with large acceptance. The interaction rates are expected to reach 10 MHz, in order to measure extremely rare probes like charm near threshold. The CBM set-up requires development of novel detector systems, trigger and data acquisition concepts as well as innovative real-time reconstruction techniques.

1.4 Quark-Gluon Plasma

Lattice QCD (LQCD) calculations suggest that a change in the state of matter (phase transition), from a color neutral hadronic system to a color conducting gas of nearly free quarks and gluons, is possible through high-energy heavy-ion interactions. Using the latest accelerator facilities like RHIC and LHC in an AB collision it is possible to produce an intermediate 'fireball' of sufficiently high energy/matter density, so that one can call it a 'state' having definite equilibrium properties. Of course the 'fireball' is not a static system and evolves with time. To talk about its thermodynamics is certainly an oversimplification. Moreover, it has been experimentally established that the 'fireball' behaves more like an imperfect fluid possessing a small but finite viscosity, and not like an ideal gas. To begin with a static idealization of the system can still be very instructive. Complexities and finer details of a real system can always be added on at a later stage.

1.4.1 Fireball Thermodynamics

At very high temperature the average kinetic energy is much higher than the rest energy of weakly interacting particles. To an excellent approximation such a system can be treated as a hot relativistic free gas. If moreover, the energy density significantly dominates over matter/baryon number density, as it is the case in RHIC or LHC, then particles and antiparticles will have nearly equal number densities and they can be created or annihilated with equal ease. In such an environment the chemical potential μ can be neglected. On the other hand color deconfinement is also possible at finite chemical potential and at a comparatively low energy density (temperature). Therefore, the color neutral hadronic phase $\leftrightarrow$ QGP phase transition can be studied under different circumstances, e.g., transition from an ideal gas of massless partons (i) to a gas of massless pions, (ii) to a nucleon gas at zero temperature, and (iii) to a system where both the temperature and the mass of the hadronic constituents are finite [29]. We shall discuss the thermodynamics of the first case with a little detail which again offers two possibilities, one for which $\mu_q = \mu_{\bar{q}} = 0$, and the other for which the

chemical potentials are not zero. For the other two cases only very brief references will be made.

• **Case (i)–massless particles with $\mu = 0$:** The number density of the ith species parton is given by,

$$n_i = \int \frac{d^3p_i}{(2\pi)^3} \frac{1}{\exp(\beta E_i) \pm 1}, \tag{1.22}$$

where $\beta = T^{-1}$ and the $+(-)$ sign corresponds to fermions (bosons). If $\beta E_i < 1$ the results are different for fermions and bosons. Setting $p_i \approx E_i$ for relativistic particles and integrating over phase space we find,

$$n_i = \frac{\zeta(3)}{\pi^2} T^3 \quad \text{for bosons,} \quad \text{and } n_i = \frac{3}{4} \frac{\zeta(3)}{\pi^2} T^3 \quad \text{for fermions} \tag{1.23}$$

where ζ is the Riemann function, $\zeta(3) \approx 1.202$. If $\beta E_i > 1$, then with increasing energy the ± 1 factor in the denominator gradually becomes insignificant, and both distributions get converted to a Maxwell-Boltzmann distribution, yielding identical results. The energy density for a free gas can be computed in a similar way

$$\varepsilon_i = \int \frac{d^3p_i}{(2\pi)^3} \frac{E_i}{\exp(\beta E_i) \pm 1}. \tag{1.24}$$

The integral results in

$$\varepsilon_i(\text{bosons}) = \frac{\pi^2}{30} T^4, \quad \text{and} \quad \varepsilon_i(\text{fermions}) = \frac{7}{8} \frac{\pi^2}{30} T^4. \tag{1.25}$$

Taking the degeneracy factor g_i associated with the ith species into account and summing over all particle species we get

$$\varepsilon = \sum_i g_i \varepsilon_i = g^* \frac{\pi^2}{30} T^4 \tag{1.26}$$

where $g^* = (g_b + \frac{7}{8} g_f)$ with g_b and g_f are the degeneracy factors, respectively for bosons and fermions. Obviously g^* depends on different degrees of freedom like charge, spin, flavor, color etc., it is an increasing function with increasing temperature. Like at $T \geqslant 100$ GeV all particles of standard model should be present and contribute to the value of g^*. If QGP can be treated as a relativistic free parton gas then the contribution to g^* from gluons comes from 2 helicity states and 8 colors, while that from each flavor of quarks comes from 3 colors, 2 spin states and 2 charge states. Depending on whether $T >$ or $T <$ the mass of a strange quark there will either be 3 (u, d, s) or 2 (u, d) flavors present in the system. Therefore,

$$\varepsilon_{qgp}(3 \text{ flavor}) \approx 47.5 \frac{\pi^2}{30} T^4, \quad \text{and} \quad \varepsilon_{qgp}(2 \text{ flavor}) = 37 \frac{\pi^2}{30} T^4 \tag{1.27}$$

is consistent with the Stefan-Boltzmann formula. Correspondingly for a free partonic gas (i) pressure $p = \varepsilon/3$, (ii) the entropy per unit volume $s = (\varepsilon + P)/T = 4\,\varepsilon/3\,T$, and (iii) the entropy per particle

$$\frac{s}{n}\Big|_{\text{bosons}} = \frac{2\,\pi^4}{45\,\zeta(3)} \approx 3.6, \quad \text{and} \quad \frac{s}{n}\Big|_{\text{fermions}} = \frac{7}{6}\,\frac{2\,\pi^4}{45\,\zeta(3)} \approx 4.2. \tag{1.28}$$

For massless hadrons (pions) ($g_{_h} = 3$) the numbers are

$$n_{_h} \;=\; 3\,\frac{\zeta(3)}{\pi^2}\,T^3; \qquad p_{_h} \;=\; \frac{\pi^2}{30}\,T^4 \tag{1.29}$$

In the framework of 'Bag model' for a QGP state comprised of (u, d, g)

$$p_{qgp} = 37\,\frac{\pi^2}{90}\,T^4 - B \tag{1.30}$$

which under critical condition (maximum pressure) will be equal to $p_{_h}$,

$$p_{_h}(T_{_c}) = p_{qgp}(T_{_c}) \quad \Rightarrow \quad T_{_c} = \left(\frac{90}{34\,\pi^2}\,B\right)^{1/4} \approx 0.72\,B^{1/4} \tag{1.31}$$

Taking the Bag constant (B) for normal hadronic matter $B^{1/4} \approx 200$ MeV/fm^3, one gets $T_{_c} \approx 144$ MeV at $\mu = 0$.

Figure 1.7(a) shows the calculated energy density ε as a function of temperature T [30]. At the critical temperature $T_{_c} \sim 170$ MeV, the energy density changes rapidly, indicating a rapid increase in the effective degrees of freedom. At $T_{_c}$ not only deconfinement occurs but also chiral symmetry is restored. The pressure variation with temperature is given in Fig. 1.7(b), where it can be seen that in comparison with the rapid increase of energy density, p/T^4 increases at a slower rate. Therefore the pressure gradient in the system ($dp/d\varepsilon$) is significantly reduced during phase transition.

• **Case (i)–massless particles with $\mu \neq 0$:** For non-zero chemical potential one should consider the 'grand potential'

$$\Omega(T,\,V,\,\mu) = -T\,\ln Z(T,\,V,\,\mu) = E \;-\; T\,S - \mu\,N = -p\,V \tag{1.32}$$

where the 'grand partition function'

$$Z(T,\,V,\,\mu) = \text{Tr}\,\exp\left[\frac{\widehat{H} - \mu\,\widehat{N}}{T}\right] = \exp\left[-\frac{\Omega(T,\,V,\,\mu)}{T}\right] \tag{1.33}$$

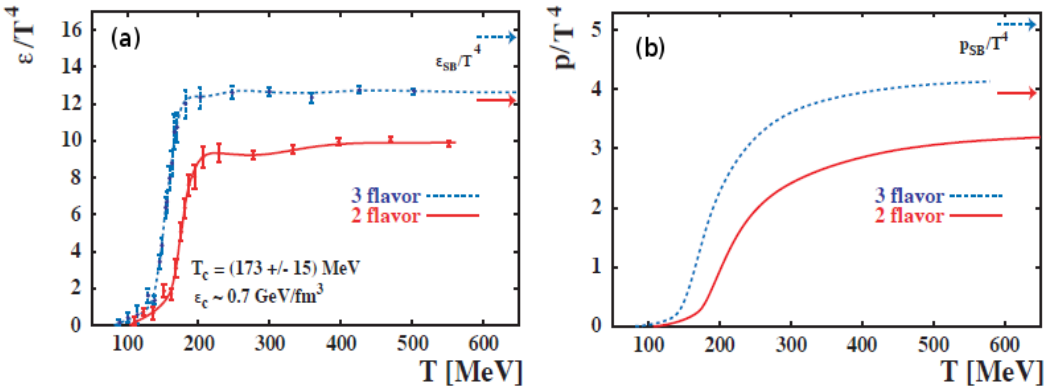

Figure 1.7: (a) Nuclear matter energy density and (b) pressure as a function of temperature from lattice calculation [30]. The arrows in the diagrams indicate the ideal Stefan-Boltzmann values.

and the relevant thermodynamic parameters are,

$$n = \frac{1}{V}\frac{\partial(T\,\ln Z)}{\partial\,\mu}, \quad p = \frac{\partial(T\,\ln Z)}{\partial\,V}, \quad s = \frac{1}{V}\frac{\partial(T\,\ln Z)}{\partial\,T} \quad \text{and} \quad \varepsilon = \frac{T}{V}\frac{\partial(T\,\ln Z)}{\partial\,T} + \mu\,n$$

In terms of the occupation number distribution functions

$$\Omega = gVT\int\frac{d^3\,p}{(2\pi)^3}\,\ln\left[1\,\pm\,\exp\left\{-(E-\mu)/T\right\}\right] \tag{1.34}$$

For massless bosons (e.g., pions and gluons) one can still assume chemical potential to be zero. Also assuming that q and $\overline{q}$ are always produced in pairs one can set $\mu_q = \mu_{\overline{q}}$. The integral that needs to be evaluated is therefore,

$$\begin{aligned} T\,\ln Z &= \frac{g_f V}{6\pi^2}\int p^3\left[\frac{1}{\exp\left\{(E-\mu_q)/T\right\}+1} + \frac{1}{\exp\left\{(E+\mu_q)/T\right\}+1}\right]d^3p \\ &= g_f V\left\{\frac{7\pi^2}{360}\,T^4 + \frac{\mu_q^2}{12}\,T^2 + \frac{\mu_q^4}{24\pi^2}\right\}. \end{aligned} \tag{1.35}$$

Adding up the gluon term the total partition function for a massless quark-gluon systems comes out to be

$$\begin{aligned} T\,\ln Z|_{qgp} &= \frac{g_b V}{90}\,\pi^2\,T^4 + g_f V\left\{\frac{7\pi^2}{360}\,T^4 + \frac{\mu_q^2}{12}\,T^2 + \frac{\mu_q^4}{24\pi^2}\right\} \\ &= V\left(\frac{37\,\pi^2}{90}\,T^4 + \mu_q^2\,T^2 + \frac{\mu_q^4}{2\,\pi^2}\right). \end{aligned} \tag{1.36}$$

Now the relevant thermodynamic parameters like, the net quark number density:

$$n_q = \left(\frac{T}{V}\right)\frac{\partial\,\ln Z|_{qgp}}{\partial\mu_q} = 2\mu_q\left(T^2 + \frac{\mu_q^2}{\pi^2}\right), \tag{1.37}$$

the energy density:

$$\varepsilon_{_{qgp}} = \left(\frac{T^2}{V}\right) \frac{\partial}{\partial T} \ln Z|_{_{qgp}} + \mu_{_q}\, n_{_q} = \frac{37\,\pi^2}{30}\, T^4 + 3\,\mu_{_q}^2\, T^2 + \frac{3\,\mu_{_q}^4}{2\,\pi^2}, \tag{1.38}$$

the pressure:

$$P_{_{qgp}} = \frac{T \ln Z|_{qgp}}{V} = \frac{37\,\pi^2}{90}\, T^4 + 3\,\mu_{_q}^2\, T^2 + \frac{3\,\mu_{_q}^4}{2\,\pi^2}, \tag{1.39}$$

and finally the entropy density

$$s_{_{qgp}} = \frac{\partial T \ln Z|_{_{qgp}}}{\partial T} = \frac{74\,\pi^2}{45}\, T^3 + 2\,\mu_{_q}\, T, \tag{1.40}$$

can easily be obtained. On the other hand the total number density of an ideal gas of massless quark, antiquark and gluons comes out as

$$n_{_{qgp}} = \frac{34\,\zeta(3)}{\pi^2}\, T^3 + 2\,\mu_{_q}^3, \tag{1.41}$$

and therefore, the ratio of the dominating terms proportional to T^3 is

$$\frac{s_{_{qgp}}}{n_{_{qgp}}} = \frac{74\,\pi^4}{45 \cdot 34\,\zeta(3)} \approx 3.92. \tag{1.42}$$

On the other hand for massless pions the corresponding numbers are:

$$\varepsilon_{_\pi} = \frac{\pi^2}{10}\, T^4, \qquad P_{_\pi} = \frac{\pi^2}{30}\, T^4, \qquad n_{_\pi} = \frac{3\zeta(3)}{\pi^2}\, T^3, \qquad s_{_\pi} = \frac{2\pi^2}{15}\, T^3, \tag{1.43}$$

and the ratio $s_{_\pi}/n_{_\pi} \approx 3.6$, is only $\sim 9\%$ smaller than the QGP state, even though the plasma has a larger degree of freedom. Looking at the enegy density and/or pressure expressions it is also evident that whether confined within a hadron or within a larger bag, a phase transition requires equal pressure across the transition region. Hence additional positive terms in the form of a potential energy has to be added / subtracted to the respective pion gas expressions and the energy density / pressure of a QGP state confined within a bag will be: $\varepsilon_{_{QGP}} = \varepsilon_{_{qgp}} + B$ and $P_{_{QGP}} = P_{_{qgp}} - B$. With a latent heat $L = 4B$ the phase transition is going to be of first order.

• **Case (ii)–nucleon gas at $T = 0$:** This situation is relevant in the context of the interior of a compact star. We have a QGP state with

$$\varepsilon_{_{QGP}} = \frac{3\mu_{_q}^4}{2\pi^2} - B, \qquad P_{_{QGP}} = \frac{\mu_{_q}^4}{2\pi^2} + B, \qquad n_{_{QGP}} = \frac{2\mu_{_q}^3}{\pi^2}, \qquad s_{_{QGP}} = 0. \tag{1.44}$$

The nucleons constitute a degenerate Fermi gas at $T = 0$ for which

$$T \ln Z|_{_N} = \frac{g_{_N} V}{6\pi^2} \int_0^\infty \frac{k^4\, dk}{E} \frac{1}{\exp[E-\mu]/T + 1}, \tag{1.45}$$

where the nucleon degeneracy factor $g_{_N} = 2$ (spin) $\times$ 2 (isospin) $= 4$. The pressure $P_{_N}$, the nucleon number density $n_{_N}$ and the energy density $\varepsilon_{_N}$ for such a system are given as

$$\begin{aligned} P_{_N} &= \frac{M^4}{6\pi^2}\left[r\sqrt{r^2-1}\left(r^2-\frac{5}{2}\right)+\frac{3}{2}\ln(r+\sqrt{r^2-1})\right], && (1.46)\\ n_{_N} &= \frac{T}{V}\frac{\partial \ln Z|_{_N}}{\partial\mu} = \frac{2M^3}{3\pi^2}\left(r^2-1\right)^{3/2}, && (1.47)\\ \varepsilon_{_N} &= \frac{T^2}{V}\frac{\partial \ln Z|_{_N}}{\partial T} = \mu\, n_{_N} - P_{_N} = \frac{2\mu}{3\pi^2}\left(\mu^2-M^2\right)^{3/2} - P_{_N}. && (1.48) \end{aligned}$$

where M = nucleon mass, μ = nucleon chemical potential and $r = \mu/M$. The nucleon number density The latent heat of transition would be

$$\begin{aligned} L &= \varepsilon_{_{QGP}} - \varepsilon_{_N} = \frac{2\mu_q^4}{\pi^2} - \frac{2\mu}{3\pi^2}\left(\mu^2-M^2\right)^{3/2}\\ &= \frac{2\mu_c}{3\pi^2} - \left[\left(\frac{\mu_c}{3}\right)^3 - \left(\mu_c^2-M^2\right)^{3/2}\right], \end{aligned} \tag{1.49}$$

where to comply with the net baryon number conservation we have to set $\mu_{_c} = 3\mu_{_q} = \mu/3$.

• **Case (iii)–finite T, finite mass:** During hadronization of a QGP state at finite temperature a range of particles, mesons, baryons and their antiparticles comprised of up, down and strange quarks are produced. The QGP can still be considered as an ideal gas of massless partons. On the hadronic side the contribution from mesons (with zero chemical potential) comes as

$$T \ln Z|_{_M} = \frac{g_{_M} V}{6\pi^2} \int_0^\infty \frac{k^4\, dk}{E} \frac{1}{\exp(E/T)-1} = \frac{g_{_M}\, V\, T^2\, m^2}{2\pi^2} \sum_{n=1}^{\infty} K_2\left(\frac{nm}{T}\right), \tag{1.50}$$

where m = meson mass, $g_{_M}$ = mesonic degrees of freedom and K_l is modified Bessel function of degree l. The pressure due to this meson gas is

$$P_{_M} = \frac{T \ln Z|_{_M}}{V} = \frac{g_{_M}\, T^2\, m^2}{2\pi^2} \sum_{n=1}^{\infty} K_2\left(\frac{nm}{T}\right). \tag{1.51}$$

As $\mu_{_M} = 0$ the energy density would be

$$\varepsilon_{_M} = 3\, P_{_M} + \frac{g_{_M}\, m^3\, T}{2\pi^2} \sum_{n=1}^{\infty} \frac{1}{n} K_1\left(\frac{nm}{T}\right), \tag{1.52}$$

and the entropy density

$$s_{_M} = 3\,\frac{P_{_M}}{T} + \frac{g_{_M}\,m^2}{2\pi^2}\,\sum_{n=1}^{\infty}\frac{1}{n}\,K_1\left(\frac{nm}{T}\right). \tag{1.53}$$

Correspondingly, the baryon and antibaryon contributions are

$$\begin{aligned} T\ln Z_{_B} &= \frac{g_{_B}\,V}{6\pi^2}\int_0^{\infty}\frac{k^4\,dk}{E}\,\left[\frac{1}{\exp\{(E-\mu_{_B})/T\}+1}+\frac{1}{\exp\{(E+\mu_{_B})/T\}+1}\right] \\ &= \frac{g_{_B}M^2T^2V}{2\pi^2}\sum_{n=1}^{\infty}\frac{(-1)^{n-1}}{n^2}K_2\left(\frac{nm}{T}\right)\times[\exp(n\mu/T)+\exp(-n\mu/T)] \end{aligned} \tag{1.54}$$

the pressure

$$P_{_B} = \frac{g_{_B}\,M^2\,T^2}{2\pi^2}\,\sum_{n=1}^{\infty}\frac{(-1)^{n-1}}{n^2}\,K_2\left(\frac{nm}{T}\right)\,\times\,[\exp(n\mu/T)+\exp(-n\mu/T)]\,, \tag{1.55}$$

the number density

$$n_{_B} = \frac{g_{_B}\,M^2\,T}{2\pi^2}\,\sum_{n=1}^{\infty}\frac{(-1)^{n-1}}{n}\,K_2\left(\frac{nm}{T}\right)\,\times\,[\exp(n\mu/T)-\exp(-n\mu/T)]\,, \tag{1.56}$$

the energy density

$$\begin{aligned} \varepsilon_{_B} &= \frac{T^2}{V}\,\frac{\partial\ln Z_{_B}}{\partial T}+\mu_{_B}\,n_{_B} \\ &= 3P_{_B}+\frac{g_{_B}M^3T}{2\pi^2}\sum_{n=1}^{\infty}\frac{(-1)^{n-1}}{n}K_1\left(\frac{nm}{T}\right)\times[\exp(n\mu/T)+\exp(-n\mu/T)] \end{aligned} \tag{1.57}$$

and finally the entropy density

$$s_{_B} = 3\frac{P_{_B}}{T}+\frac{g_{_B}\,M^3}{2\pi^2}\,\sum_{n=1}^{\infty}\frac{(-1)^{n-1}}{n}\,K_1\left(\frac{nm}{T}\right)\times[\exp(n\mu/T)+\exp(-n\mu/T)]\,. \tag{1.58}$$

Both the meson and baryon contributions are to be included into the hadron gas. Setting $\mu_{_c} = 3\mu_{_q} = \mu_{_B}$ and $T = T_{_c}$ at the phase boundary one gets

$$P_{QGP} = P_{_B} + P_{_M} \qquad \text{and} \qquad L = \varepsilon_{QGP} - (\varepsilon_{_B}+\varepsilon_{_M})\,. \tag{1.59}$$

However, the fireball is a dynamically evolving system. Therefore, instead of using a static thermodynamic description, hydrodynamical models are always preferred.

1.4.2 The Hydrodynamics

Bulk of the particles produced (about 95%) in AB collisions are thermal pions ($p_{_\perp} < 2$ GeV/c) associated with 'soft' processes. Their distribution will give us a first insight to the overall collision dynamics. The extreme view of complete stopping of the colliding nuclei was implicit in Fermi's work [31] and described in the hydrodynamical model of Landau [32]. The entire initial longitudinal energy is inelastically transferred to produced particles and redistributed both in the transverse and longitudinal dimensions. In a symmetric AA collision Landau's model not only assumes complete stopping of the reacting nucleons, but also an accumulation of matter and energy in a single mid-rapidity fireball that subsequently experiences hydrodynamical expansion like an ideal one-dimensional fluid. In this model the maximum achievable energy density is

$$\varepsilon_{\max} = \frac{E_{cm}}{V_{_A}} = \frac{3\,\gamma_{cm}\,\sqrt{s}\,N_{part}}{4\pi\,R^3} = \frac{3\,s\,N_{part}}{4\pi\,m_{_N}\,R^3}, \tag{1.60}$$

while the dispersion of the Gaussian follows, $\sigma^2 \propto \ln(\sqrt{s}/2m_{_N})$. A perfect fluid does not have any viscosity and therefore, does not produce any entropy. Using simple thermodynamics of an ideal gas of massless particles one can write

$$s \propto \varepsilon^{3/4} \qquad \text{and} \qquad T \propto \varepsilon^{1/4} \tag{1.61}$$

As the initial energy density $\varepsilon \propto E_{cm}^2$, and as according to the black body formula the number of produced particles is proportional to the entropy, the produced particle number comes out as, $N \propto E_{cm}^{1/2}$. As a consequence of initial Lorentz contraction, the intermediate fireball evolves predominantly in the longitudinal direction. Landau's picture suffers from a limitation that the colliding nuclei must possess unrealistically large stopping power, which they don't have. However, recent works show that combining a quark constituent picture with Landau's hydrodynamical model, the $\sqrt{s}_{_{NN}}$ dependence of important global parameters like (i) pseudorapidity density of charged particles produced per participant pair, and (ii) charged particle mean multiplicity per participant pair, both measured in the midrapidity region of central AA collisions can be very accurately predicted over a wide collision energy range, $\sqrt{s}_{_{NN}}$ = a few GeV to a few TeV [33]. With increasing $\sqrt{s}_{_{NN}}$ while the midrapidity particle density is found to obey a linear-log increase, the multiplicity data increases following a second-order log-polynomial fit.

With increasing collision energy a non-Gaussian central peak develops into a double hump structure in the net baryon rapidity distribution that widens toward RHIC and LHC energies leaving a plateau in the mid-rapidity, thereby maintaining a boost invariance within the central rapidity region. The observed total $E_{_\perp}$ amounts only to a fraction (about 60%) of

its maximum value $\left(E_{\perp}^{max}\right)$ that can result from complete stopping. The remaining part is therefore, used to sustain the longitudinal motion. As a rsult the central fireball fixed in the CMS gets converted to a logitudinally extended firetube i.e., a cylindrical volume containing high energy density, based on relativistic hydrodynamics an idea that was first introduced by Bjorken [19]. Hydrodynamics is a macroscopic approach to describe the dynamical evolution of the expansion stage of a heavy-ion collision. It is assumed that shortly after the collision the strongly interacting matter reaches a state of local thermal equilibrium and subsequently expands adiabatically. The evolution of the system is determined by its initial conditions and the equation of state (EoS) [34, 35], which relates the energy and the baryon density to the pressure exerted by the system, and which is subject to the constraints of local conservation of energy, momentum, and currents (e.g., baryon number). The energy-momentum tensor $T^{\mu\nu}$ and the current density j^{μ} of an ideal non-dissipative fluid are given by,

$$T^{\mu\nu}(x) = [\varepsilon(x) + p(x)]u^{\mu}(x)u^{\nu}(x) - g^{\mu\nu}p(x), \tag{1.62a}$$

$$j^{\mu}(x) = n(x)u^{\mu}(x), \tag{1.62b}$$

where $\varepsilon(x)$ is the energy density, $p(x)$ the pressure, and $n(x)$ the conserved number density at point x and $u^{\mu}(x) = \gamma(x)\,[1, \overline{v}(x)]$ is the local four velocity of the fluid. Note that $u^{\mu}\,u_{\mu} = 1$. The conservation laws are written in the form of continuity equations,

$$\partial_{\mu}T^{\mu\nu}(x) = 0 \quad \text{and} \quad \partial_{\mu}j^{\mu}(x) = 0. \tag{1.63}$$

The EoS describes how macroscopic pressure gradients generate collective flow. One has to solve,

$$\partial_{\mu}\left[(\varepsilon + P)\;u^{\mu}\,u^{\nu} - g^{\mu\nu}\,P\right] = 0. \tag{1.64}$$

Multiply with u_{ν} and use $u_{\nu}\,\partial_{\mu}\,u^{\nu} = 0$ to write

$$u^{\mu}\partial_{\mu}\,\varepsilon + (\varepsilon + P)\;\partial_{\mu}u^{\mu} = 0. \tag{1.65}$$

Dropping the transverse co-ordinates one can write,

$$t = \tau\cosh y \quad \text{and} \quad z = \tau\sinh y \tag{1.66}$$

in terms of the spacetime rapidity (y), so that $u^{\mu} = (t/\tau,\, 0,\, 0,\, z/\tau)$, where the Lorentz invariant proper time $\tau = t/\gamma = \sqrt{t^2 - z^2}$ and $u_{z} = z/t = \tanh y$ is the longitudinal velocity. The Bjorken equation

$$\frac{\partial\varepsilon}{\partial\tau} + \frac{\varepsilon + P}{\tau} = 0$$

can now be arrived at. One can also use $\varepsilon = \lambda\,P$, where $\lambda = dP/d\varepsilon = c_s^2$, the elastic wave

velocity in the medium, is a constant e.g., $c_s^2 = 1/3$ for an ideal gas of massless particles. Therefore,

$$\frac{\partial \varepsilon}{\partial \tau} + \frac{(1+\lambda)\,\varepsilon}{\tau} = 0 \quad \Rightarrow \quad \varepsilon(\tau_f) = \varepsilon(\tau_i) \left(\frac{\tau_i}{\tau_f}\right)^{1+\lambda}. \tag{1.67}$$

From thermodynamics one can write

$$\varepsilon + P \;=\; T\,s \;+\; \mu_{_B}\,n_{_B}. \tag{1.68}$$

For zero net baryon density,

$$d\varepsilon = T\,ds \;\text{ and }\; s \;=\; \frac{(1+\lambda)\,\varepsilon}{T} \quad \Rightarrow \quad s(\tau_f) \;=\; s(\tau_i) \left(\frac{\tau_i}{\tau_f}\right) \tag{1.69}$$

Also,

$$T\,\frac{ds}{d\tau} \;=\; \frac{d\varepsilon}{d\tau} \;=\; -\frac{(1+\lambda)\,\varepsilon}{\tau} \;=\; -\frac{s\,T}{\tau} \tag{1.70}$$

$$\Rightarrow \quad \frac{ds}{d\tau} + \frac{s}{\tau} \;=\; 0 \qquad \Rightarrow \quad T(\tau) \;=\; (1+\lambda)\,\frac{\varepsilon(\tau)}{s(\tau)} \;=\; T(\tau) \left(\frac{\tau_i}{\tau_f}\right)^{\lambda} \tag{1.71}$$

A phase transition from the QGP phase to a hadron gas causes a softening of the EoS. As the temperature crosses the critical temperature, the energy and entropy densities increase rapidly while the pressure rises slowly. The derivative of pressure to energy density (p/ε) has a minimum at the end of the mixed phase, known as the softest point. The diminishing driving force slows down the build-up of flow. The initial conditions which are input parameters, describe the starting time of the hydrodynamic evolution and the relevant macroscopic density distributions at that time. The hydrodynamic evolution is terminated by implementing the freeze out condition which describes the breakdown of local equilibrium due to decreasing local thermalization rates. In noncentral collisions, driven by its internal asymmetric pressure gradients, the system will expand more strongly in the direction of the reaction plane than perpendicular to the reaction plane. As time evolves, the system becomes less and less deformed. To estimate the initial energy density of a Bjorken-type fluid element therefore, one has to go to the fluid rest frame. All particles are originating from a cylindrical volume of cross-section area $\mathcal{A}$, which actually is the overlap area of the interacting nuclei, and of length $u_z\,t$. We concentrate on a thin slab of thickness dz centered between the two pancake-like moving nuclei (Fig. 1.8). The point of impact of the collision is assumed to be the origin ($z = 0$) of our frame of reference. Therefore $dz = \tau\,\cosh y\,dy$, and ignoring collisions between the produced hadrons, one can write the energy density as,

$$\varepsilon_{_{BJ}} = \frac{\Delta E}{\Delta V} = \frac{E}{\mathcal{A}}\,\frac{dN}{dz} = \frac{m_{_\perp}}{\pi\,R^2\,\tau}\,\frac{dN}{dy} = \frac{1}{\pi\,R^2\,\tau}\,\frac{dE_{_\perp}}{dy}. \tag{1.72}$$

Taking the proper time $\tau \sim 1$ fm/c and (dN/dy) to be the central rapidity density of

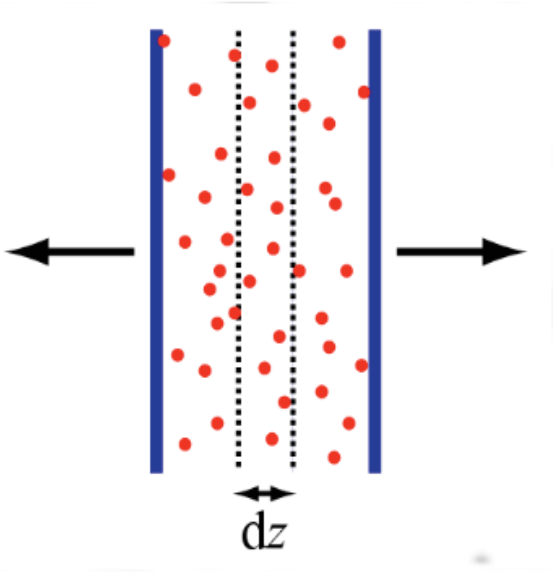

Figure 1.8: Bjorken model of nucleus-nucleus collision.

produced particles, this relation was first derived by Bjorken [19]. However, a perfect fluid must undergo an isentropic expansion, and the entropy of the expanding fireball S should be a conserved quantity. In terms of entropy density $s = S/V$ for one-dimensional expansion, therefore to compensate the Lorentz contraction a relation like $s_i\,\tau_i = s_f\,\tau_f$ should hold between an initial (τ_i) and final (τ_f) proper time. As it will be shown later, for massless particles, $\varepsilon = g\,\frac{\pi^2}{30}T^4$ and $s \propto T^3$, where T is the temperature and g is number of the degrees of freedom. Correspondingly,

$$T_i^3\,\tau_i = T_f^3\,\tau_f \;\Rightarrow\; \tau_f = \tau_i\left(\frac{T_i}{T_f}\right)^3 \quad \text{and} \quad \varepsilon_f = \varepsilon_i\left(\frac{\tau_i}{\tau_f}\right)^{4/3} \tag{1.73}$$

which is in contradiction with Bjorken's formula, $\varepsilon_{BJ} \sim \tau^{-1}$. The energy density formula should therefore, be modified as

$$\varepsilon = \frac{1}{\pi\,R^2\,\tau_0}\,\frac{dE_\perp}{dy}\left(\frac{\tau_f}{\tau_i}\right)^{1/3} = 2\,\varepsilon_{BJ}. \tag{1.74}$$

1.4.3 QCD Phase Diagram

The phase diagram (pressure vs temperature) of water has three broad regions separated by phase transition lines, the triple point where all three phases coexist, and the critical point where the vapor pressure curve terminates and two distinct coexisting phases, namely liquid and gas, become identical. Such a diagram is shown in the left panel of Fig. 1.9. In contrast the QCD phase diagram is known only schematically [11]. In high-energy AB collisions we expect two transitions to take place, one is the color deconfinement and the

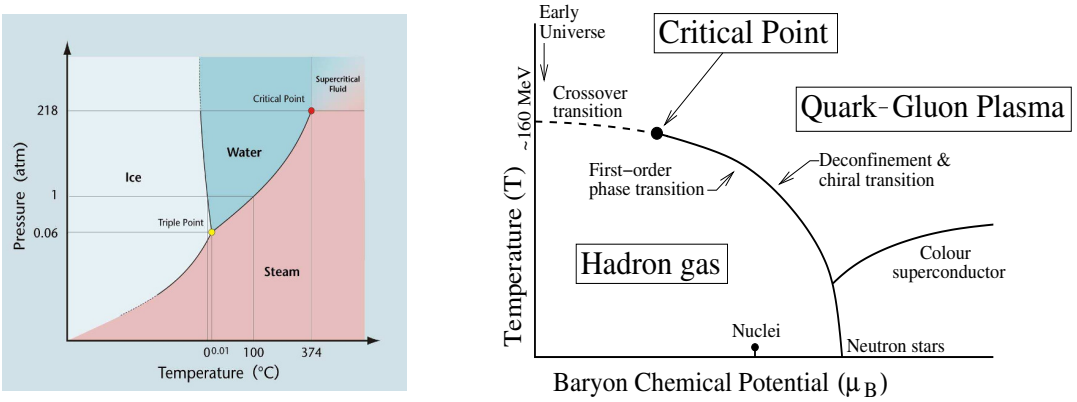

Figure 1.9: Phase diagram of water (left). A schematic phase diagram of QCD matter (right).

other is the restoration of chiral symmetry. The order parameters are the Polyakov loop for the former and quark condensate for the latter, neither of which can unfortunately be measured in experiments. LQCD and common wisdom however suggest that both should occur at a common T_c at least at small μ_B. LQCD also predicts a crossover transition around $T \sim 150 - 170$ MeV for vanishing μ_B. As mentioned, there are two extreme conditions of QGP to hadron phase transition, (i) at high temperature and at zero net baryon density, and (ii) at high baryon density and at zero temperature. For a system in between these two limits, there is a pressure arising from the thermal motion of the particles as well as from the degeneracy of the fermion gas. Thus, for a system having non-zero pressure and temperature, the critical temperature shall be placed in between the two extreme limits. The study of the intermediate region of the phase diagram is quite complicated as perturbation theory cannot be applied to QCD near T_c, and furthermore at finite baryon density the usual lattice approach fails [36, 37]. Therefore, one of the major objectives of high-energy heavy-ion physics is to explore the QCD phase diagram in the various temperatures and baryon density regions so as to confirm the existence of new phase of nuclear/partonic matter. Arguments based on a variety of other models indicate a first order phase transition as a function of T at finite μ_B, which one expects to terminate at a critical point [37]. The existence of the critical point, however, is not yet established in experiments. Apart from the region of color neutral hadrons at the low T and low μ_B, and the region of quarks and gluons at high T and high μ_B, there is also a region characterized by the color superconductivity, at high μ_B and low T. However, precise boundaries separating these regions are not yet known. Mapping the QCD phase diagram at least at a quantitative level, is possible by using LQCD. Although it allows first-principle calculations, there are technical difficulties for non-vanishing μ_B. There exist however, various other effective theories and phenomenological models [38] which form the basis of the schematic QCD phase diagram (μ_B against temperature T), shown very naively in the right panel of Fig. 1.9. Experimental tools available to explore such a diagram

are the relativistic heavy-ion accelerators. Apart from the terrestrial facilities, astronomy of neutron stars can also shed some light on the low T and high μ_B region of the phase diagram. Unlike a system in global equilibrium, here temperature and chemical potential may depend on space-time coordinates.

1.4.4 Signals of QGP

We know that the central fireball created in a high-energy AB collision expands very rapidly, and we observe as an outcome a large number of color neutral hadrons, leptons and photons streaming out of the collision debris. One needs to identify appropriate experimental tools (signals) for detecting the quark-gluon plasma, and to study its properties, if it is at all created. The problems associated with such a task are, (i) the volume filled up with QGP is at most several fermi in diameter and (ii) the time scale for which such a state exists $\sim$ 5 to 10 fm/c [39, 40]. Moreover, signals of QGP are often shadowed under a huge background particles emitted from the hot hadronic gas. Different types of experimental probes have been put forward to examine different stages of the hot and dense matter as it expands and evolves back to normal color neutral hadronic state. There are some soft probes and some hard probes [35, 36]. Arranging in increasing order of hardness they are, (i) global observables–multiplicity distribution and rapidity distribution, (ii) geometry of emitting source–HBT, impact parameter via zero-degree energy flow, (iii) early state collective effects–elliptic flow, (iv) chiral symmetry restoration–neutral to charge ratios, resonance decays, (v) fluctuation phenomena–event-by-event particle composition and spectra, (vi) degrees of freedom as a function of T–hadron ratios and spectra, dilepton continuum, direct photons, (vii) deconfinement–charmonium and bottomonium spectroscopy, (viii) energy loss of partons in QGP–jet quenching, high $p_\perp$ spectra, open charm and open beauty. A qualitative discussion on some of these are furnished below.

• **Hanbury-Brown–Twiss (HBT) Effect:** Identical particle correlation or interferometry, provides information on the reaction geometry, and hence provides important information about the spacetime dynamics and system lifetime of nuclear collisions. The information about the spacetime structure of the particle emitting source created in AB collisions obtained from the measured particle momenta, can be extracted by the method of the so called 'two-particle intensity interferometry techniques' also called the 'Hanbury-Brown–Twiss' (HBT) effect [41, 42]. The method was initially developed to measure the angular size of distant stars [43]. The two-particle correlation arises from the interference of particle wave-functions, where interference is defined as a phenomenon associated with the superposition of two or more waves. Such correlation depends on whether the particles are bosons or fermions. Also the degree of interference depends on the degree of coherence of the emitting

source of particles produced in such collisions, which reaches a maximum for a completely incoherent source. HBT is a useful method to understand the crucial reaction mechanism and equation of state (EoS) of the particle emitting source in relativistic heavy-ion collisions [44] where the QGP is expected to be formed. LQCD predicts a very soft EoS near about the QCD critical point ($T_c = 173 \pm 15$ MeV), and a sudden decrease in $dp/d\varepsilon$ ($= c_s^2$) value from what is obtained in the $T > 2T_c$ region [30], c_s being the speed of sound in QCD medium.

• **Collective Flow:** The particles produced in a high energy AB collision show a high degree of collective behavior which is termed as flow [45]. Due to spatial asymmetry of the overlapping volume of the colliding nuclei, the pressure gradient generated at an early stage of collision leads to an anisotropic transverse collective flow during the expansion of the hot and dense matter [46]. By characterizing asymmetric azimuthal distribution of particles emitted from non-central collisions, we can understand the extent of this outward pressure. When decomposed into Fourier components the invariant azimuthal distribution

$$\frac{d^3N}{d^3p} = \frac{1}{2\pi E\, p_\perp} \frac{d^2N}{dp_\perp\, dy} \left[1 + \sum_{i=1}^{N} 2\, v_n \cos\{n(\phi - \psi_{RP})\}\right] \tag{1.75}$$

has many non-zero coefficients. Here E, $p_\perp$, y, and ϕ are, respectively the energy, transverse momentum, rapidity and azimuthal angle of the produced particle, and ψ_{RP} is the azimuthal angle of the reaction plane which is defined as the plane spanned by the impact parameter vector and the beam direction. The first coefficient v_1 measures the 'direct flow' while the second coefficient v_2 is called the 'elliptic flow' and so on. The v_2 coefficient, almost in all high-energy AB collisions, is found to be the largest [47]. Such type of Fourier decomposition really measures particle emission directly correlated with the orientation of the density gradients as shown by the fact that v_2 for all charged particles at low transverse momenta scales linearly with the *eccentricity* of the overlap region of the colliding nuclei [48]. In the high-$p_\perp$ region hadronization occurs through fragmentation, whereas in the medium-$p_\perp$ region it is modeled by quark recombination or coalescence. The phenomenon of constituent quark number scaling provides experimental support to this model. When scaled by the constituent quark number, the v_2 against $E_\perp$ curves merge into one universal curve, suggesting that elliptic flow actually develops at the quark level, and hadrons form through merger of constituent quarks.

• **Chiral Symmetry Restoration:** The approximate 'chiral symmetry' of QCD is spontaneously broken by the existence of a quark condensate in vacuum [39]. Due to large energy deposit in the collision zone of the relativistic collisions, if the QGP is formed then the medium would possess chiral symmetry. But the rapid expansion at earlier times suddenly reduces the temperature down, and the symmetry is spontaneously broken [49]. Lattice

simulations predict a very rapid drop of the scalar quark condensate $\langle q\bar{q}\rangle$ from its vacuum value to almost zero in a narrow temperature region around T_c. The temporary restoration of chiral symmetry in nuclear collisions may result in the formation of domains of disoriented chiral condensate [40].

• **Event-by-event Fluctuation:** Another set of global observables are related to *fluctuations*, which are of fundamental importance for studying perturbation to a thermodynamic system [39]. Several thermodynamic quantities show varying fluctuation patterns when the system undergoes a phase transition [50]. In the study of phase transition the measurement of particle number density, energy and charge fluctuations are relevant. Event-by-event fluctuations of thermodynamic quantities measured in high-energy heavy-ion collisions provide a reasonable framework for studying the nature of the QGP to hadron phase transition in the laboratory [51]. As for example, the fluctuations in the total charge contained in an ideal gas sub-system comprising of $N\,(=N_+ + N_-)$ particles is given by, $\left\langle \delta Q^2 \right\rangle = q^2 \left\langle N_+ + N_- \right\rangle$ where $N_\pm$ are the number of positively and negatively charged particles. Obviously the above quantity is sensitive to the square of the charge q of the constituent particles, which should be smaller for a quark-gluon system than a color neutral hadronic system. The ration of charge fluctuation per entropy is four times larger in a pion gas than that in a 2-flavor QGP. Even if the contribution from hadronic resonances is taken into account the above factor reduces to three, thereby leaving a genuine signal for a QGP state.

• **Strangeness Enhancement:** The production of hadrons containing s quarks is normally suppressed in hadronic reactions compared with the production of hadrons containing only u and d valence quarks. This suppression increases with growing strangeness content of the produced hadrons. The theoretical studies have shown that strangeness is produced rapidly in the collisions of thermalized gluons, within the deconfined state formed in heavy-ion collisions [52, 53]. When QGP is formed, the production of hadrons carrying s quarks is expected to saturate because of s quark content of the plasma is rapidly equilibrated by $s\bar{s}$ pair production in the interaction between two gluons. So the yield of multi-strange baryons and strange antibaryons is predicted to be strongly enhanced [54] in a QGP medium. The deconfined state of QGP breaks up in a fast hadronization process with the enhancement of strange hadrons and strange anti-baryons, along with the rise of valence quark content of hadrons produced as the predicted property of deconfined phase [54]. This occurs due to the breakup of strangeness rich deconfined states (or hadronization), where several strange quarks are formed before and the independent reactions can combine into a multi-strange hadron.

• **Dilepton production:** Leptons are produced at an early stage of the collision and they can probe the very interior of the hottest stage of evolution of the fireball. The produced lepton pairs ($l^\pm$) carry information regarding the thermodynamical state of the medium at

the moment of their production. The production rate and the momentum distribution of the dilepton pairs depend on the momentum distribution of quarks and antiquarks present in the plasma, which in turn are governed by the thermodynamic condition [36]. In high energy AB collisions a probable formation of QGP is not the only source of dilepton production. There exist other processes, like the Drell-Yan process, which is important for large values of the invariant mass of the $l^{\pm}$ pair [36, 55]. In the Drell-Yan process a valence quark of a nucleon of one of the colliding nuclei interacts with a sea antiquark of a nucleon belonging to the other nucleus. The $q\bar{q}$ pair annihilates to form a virtual photon (γ^*), which subsequently decays into a $l^{\pm}$ pair. In addition a large fraction of the dilepton yield arises from the decay of long lived states, such as the neutral pions, eta, or the omega mesons. These resonances decay well outside the hot and compressed region and therefore, in order to extract information regarding the properties of hot and dense matter, a detailed analysis of the dilepton spectra, like in medium modification of hadron properties, is needed. In the low mass region, below the ϕ-meson mass limit, the most important production channels are, (i) delayed decay of $\eta, \Delta, \omega, a_1$ and (ii) direct decay of the vector mesons such as ρ, ω and Φ. Therefore, in order to separate out the portion of invariant mass spectrum of $l^{\pm}$ due to QGP, it is essential to analyze the contribution from all other sources of dilepton production [55].

• **Thermal Photon production:** Photons are emitted throughout the expansion process, but their production is expected to be weighted more toward the hot and dense early stages of the collision. The photon production schemes in heavy-ion collision are complex in nature, and they may grossly be classified into four groups [56] namely, (i) the hard partonic scattering produces photons that falls off at large transverse momentum–such production rates can be calculated by making use of the perturbative QCD; (ii) photons are emitted in the collisions between quarks and gluons in the QGP medium–the energy spectrum of such photons is damped exponentially having a long tail extended up to several GeV; (iii) during hadronization the produced hadrons collide with other hadrons and resonances (ρ, ω)–such collisions may emit photons with energy values ranging from several hundred MeV to several GeV; (iv) photons can also be the decay products of the neutral mesons like π^0, η etc., emerging at the end of the thermal evolution and have energies in the range of $< 10^2$ MeV. Note that π^0 and η mesons can also be produced in hard partonic scattering at the early stage of the collision having several GeV of energy, and can subsequently decay into high $p_{\perp}$ photons. These photons together with those mentioned in category (i) appears as a background to the thermal photons produced in category (ii) and (iii), which carry the information of the hot and dense matter produced in high-energy AB collisions [57].

• **Charmonium Production:** If a J/ψ particle, a bound state of $c\bar{c}$, is placed in QGP, the color charge of c will be screened by the quarks, antiquarks and the gluons on the plasma. The basic mechanism for deconfinement in the dense QGP is the Debye screening of the

quark color charge. The effect of Debye screening will modify the the long-range Coulomb potential into a short-range Yukawa potential with the range given by Debye screening length λ_D. Note that in a QGP the string tension between two quarks κ vanishes. When the screening radius becomes less than the binding radius of a quark-antiquark system, which means that it becomes less than the hadron radius, the confining force can no longer hold the quark-antiquark pair together and hence deconfinement sets in. The J/ψ has a radius of about 0.2 fm [58]. which is much smaller than the normal hadronic scale $\lambda_{QCD}^{-1} \approx 1$ fm. having a binding energy of 0.6 GeV which is larger than $\lambda_{QCD} \approx 0.2$ GeV. λ_{QCD} is called the QCD scale parameter to be determined from experiments. In AB collisions the J/ψ particles are produced in the initial stage of hard scattering. The suppression of J/ψ production in a quark-gluon plasma occurs because a $c\bar{c}$ pair formed by fusion of two gluons from the colliding nuclei cannot bind inside the quark-gluon plasma. Hence the effect of plasma will make the J/ψ unbound, thus the suppression of J/ψ production could be a possible signature of QGP formation [59]. There is however, an alternative proposition about charm production in AB collisions. As a hard process, charm production increases with collision energy at a much faster rate than that of the light quarks. At sufficiently high-energy the produced medium will therefore, contain more charm quarks than present in a QGP at chemical equilibrium. If these charm and anti-charm quarks combine at the hadronization point statistically to form charmonium states, the new combination mechanism should lead to a much enhanced J/ψ production rate, even if all primary (direct) J/ψ's are dissociated [60]. The two predictions, sequential suppression against statistical regeneration, thus represent two really contradictory viewpoints, and the LHC results should be able to substantiate either (or both) of them [61].

• **Jet Quenching:** Hard-scattered partons (quarks and gluons) produced internally in AB collisions can be used to probe the medium in which it is produced. Nucleons belonging to the colliding nuclei may interact with each other and produce partons with large transverse momenta, which subsequently fragment and emerge as jets of particles in the final state. Hard partons are produced early in the collision, and therefore, they can probe the early stages of collision. Moreover, their production rate can be calculated using perturbative QCD. Partons/jets are color carrying objects and therefore, they interact strongly and lose more energy (or get quenched) in a QGP-like medium than in a color neutral hadronic matter. Among other factors the amount of energy loss depends on the path length the jet has to travel inside the medium. The yields of high-$p_\perp$ pions and etas are found to be suppressed by a factor of about 5. Such suppressions are not seen either in d + Au or in p + Pb collisions where QGP formation is not expected, thereby ruling out suppression by cold nuclear matter [62]. These observations indicate that hard partons lose energy as they traverse the hot medium and jet suppression is therefore, a final-state effect. Jet quenching in hot dense matter can also be studied in terms of dihadron correlations as a function of

opening angle between a high-$p_\perp$ trigger and associated particles. In the azimuthal plane of AB collisions there is always an enhanced high-$p_\perp$ jet production in the near side than in the away side, a phenomenon that is absent in proton-proton or in proton-nucleus collisions. When soft (low-$p_\perp$) hadrons are included into trigger, jets appear in both near and away sides in all types of interactions.

1.5 Models of AB Interaction

In order to get a complete description of a high-energy AB collision, the QCD must be employed without any approximation. But as we know, due to the intrinsic complexities associated with the QCD, nonperturbative effects are to be treated through model calculations. Unfortunately, till date we do not have any complete model that describes all stages of space-time evolution process in an AB collision. The hadronic models, where an AB interaction is considered as a superposition of many NN interactions, try to simulate the entire history of the space-time evolution, and any deviation observed in comparison with measurement is considered as a collective effect. Models based on string fragmentation mechanism(s), parton shower cascade and transport mechanism focus on the initial pre-equilibrium stage of the interaction. Hydrodynamical model, on the other hand, mainly describes various equilibrium stages of the space-time evolution. In this section a brief description is given for some of the phenomenological models and theory that are currently being used by the heavy-ion community.

1.5.1 RQMD and UrQMD

The Relativistic Quantum Molecular Dynamics (RQMD) model is designed to give a complete description of an AB collision, that starts from the initial overlapping of the colliding nuclei and ends at the final freeze out state when strong interaction among the outgoing hadrons ceases to act. This is a semi-classical microscopic transport theory, where the incoming objects are represented by their classical trajectories and the interactions are treated stochastically [63]. The model nicely works in the BNL-AGS and CERN-SPS energy domains. At high-energy ($E_{\rm lab} > 10$A GeV) AB collisions, a Glauber type sequence of multiple scatterings is generated on the partonic level. Strings and resonances are excited in elementary NN collisions, where the strings can overlap to form chromoelectric flux tubes called called the 'ropes'. Secondary particles are produced through the fragmentation of resonances, strings and ropes. Subsequently, the fragmentation products interact with each other and also with the original nucleons, mostly via binary collisions. For this purpose a relativistic Boltzmann equation has to be solved for hadrons in the final stage of the collision.

These interactions drive the system toward equilibration and are the underlying mechanism which makes collective flow to develop even in the pre-equilibrium stage. In this model, the equilibrium pressure is simply due to an ideal gas of hadrons and resonances. The resulting equation of state in the cascade mode of RQMD is similar to the one in ref. [64].

The Ultra-relativistic Quantum Molecular Dynamics (UrQMD) [65] is based on analogous principles as the RQMD but with a vastly extended collision term. The range of applicability of UrQMD includes the SIS energy region ($\sqrt{s} \approx 2$ GeV) up to the RHIC energy ($\sqrt{s} = 200$ GeV). Currently, the model has been employed to simulate LHC events as well. In the UrQMD model the projectile and the target nuclei are treated according to a Fermi gas ansatz. In this scheme particle production at high-energy is implemented by the color string fragmentation mechanism similar to the Lund model [66]. The UrQMD code has been successfully used to reproduce the particle density distributions and the $p_\perp$ spectra of various particle species in proton-proton, proton-nucleus and AB collisions. At $\sqrt{s_{NN}} \approx 10$ GeV the model can reproduce the elliptic flow parameter reasonably well. However, the model does not incorporate the symmetry aspects of the fields associated with the identical particles, and it predicts very small HBT radii. As the UrQMD code has been utilized to generate ^{28}Si-Ag/Br event sample at 14.5A GeV incident energy that has been used in the present investigation, we shall give a detailed description of the model in Section 2.5. The advantage of using transport models like RQMD or UrQMD is that they treat the final freeze-out stage dynamically, do not make any equilibrium assumption, and describe the dynamics of a hadron gas like system very well in and out of the chemical and/or thermal equilibrium. Therefore, AB interactions where it is less likely for the intermediate 'fireball' to reach a local equilibrium, these models are very useful.

1.5.2 HIJING

Heavy Ion Jet Interaction Generator (HIJING) [67] is a MC event generator developed to study jet and associated particle production in high-energy pp, pA and AB collisions. HIJING combines a QCD inspired model for jet production with the Lund FRITIOF [66] and Dual Parton model [68] for soft processes at intermediate energies ($\sqrt{s} \lesssim 20$ GeV/nucleon), and presents a successful implementation of pQCD process in PYTHIA model [69] for hadronic collisions. The model is designed mainly to explore the range of possible initial conditions that may occur in relativistic heavy-ion collisions. Nuclear shadowing of parton (specially the gluon) structure functions and a schematic model of final state interaction of high $p_\perp$ jets in terms of an effective energy loss parameter dE/dz, have been included into the model to study the nuclear effects. To generate the initial phase space distribution for the parton cascade, the formation time for each parton is determined according to a

Lorentzian distribution with a half-width $t_f = E/m_\perp^2$, where E is the parton energy with transverse mass $m_\perp$. During the time of formation partons are considered to be part of the coherent cloud of parent nucleons and hence they do not suffer rescattering. Once the partons stop interacting, after an additional proper time of about 1.2 fm. they are converted into hadrons according to the HIJING fragmentation scheme.

1.5.3 AMPT

The AMPT (A Multi-Phase Transport) model [70] is an example of a hybrid type transport model. The initial conditions of AMPT are obtained from the HIJING that uses a Glauber formalism to determine the positions of participating nucleons. AMPT uses Zhang's Parton Cascade (ZPC) formalism [71] for fixing the scattering properties of partons. Note that the ZPC model includes only parton-parton elastic scattering with an in-medium cross section derived from pQCD along with an effective gluon screening mass taken as a parameter. After the minijet partons stop interacting, they are combined with their parent strings. The hadronization process is settled either by using the Lund fragmentation or by a quark coalescence scheme. The string fragmentation mechanism is same as that implemented in the PYTHIA program [72]. The final state hadronic scatterings are then modeled by a relativistic transport (ART) model [73]. In the AMPT model, there also exists a string melting scenario in which hadrons, that would have been produced from string fragmentation, are converted instead to valence quarks and antiquarks with their current quark masses [74]. Interactions among these partons are again described by the ZPC parton cascade model. As there are no inelastic scatterings, only quarks and antiquarks from the melted strings are present in the partonic matter. The transition from partonic matter to hadronic matter is achieved using a simple coalescence model, which combines two nearest quark and antiquark into mesons and three nearest quark(s) and/or antiquark(s) into baryons/antibaryons. The particle type is determined by the invariant mass of these partons. The users thus have a choice of using either of these two modes of particle production. In the default configuration of AMPT the energy of the so-called excited strings are not used in the partonic stage and only released in the hadronization stage, as it was implemented into the Lund string fragmentation model. On the other hand as mentioned above, in the string melting (SM) configuration of AMPT all excited strings are first converted (melted) into partons, and at the end of interaction stage the left over partons are combined into either mesons or baryons through a quark coalescence mechanism.

1.6 Multiparticle Production

A high-energy AB interaction is usually considered to be a superposition of many nucleon-nucleon (NN) collisions. In an AB collision each nucleon may rescatter several times and the produced partons from different NN collisions can also rescatter with each other before hadronization. Both these factors influence the particle production phenomena per participating nucleon in an AB interaction. In the final state a large number of particles comprising mostly of various types of hadrons, along with some photons and leptons are observed. The hadrons are created in the freeze-out stage which is a relatively late stage of the fireball expansion [75–77]. Therefore, they provide only indirect information of the intermediate equilibrated stage(s), if there is any. However, the hadrons are very abundant, they can be easily identified and their kinematic properties can be accurately measured. We can expect that there will be some rare but interesting events showing something exotic and unusual, while on the other a large majority of events will exhibit regular features e.g., a finite number of particles will come out with different energy-momentum values from each event. To extract any kind of nontrivial physics these regular events have to be subjected to rigorous statistical analysis. The particle number will vary from event to event which for a large event sample will result in a distribution of the particle multiplicity as well as distributions in terms of different kinematic variables. The primary objective of the present thesis is to analyze some of these distributions in a particular AB interaction, and therefore, in the following subsections we summarily outline some of the issues related to multiparticle production, some of which will subsequently be discussed in details.

1.6.1 Particle Density Fluctuation

The study of fluctuation of various final state observables drew an extra attention since the early days of high-energy collision experiments. Fluctuation in the density distribution of particles produced in AB collisions itself can render a lot of information on multiparticle dynamics, and this actually is the subject matter of our present investigation. Of course, there is always a trivial statistical component (noise) associated with the observed fluctuation that has to be carefully eliminated. The *nonstatistical* (also called *dynamical*) component of density fluctuation that results from some nontrivial dynamics is not yet fully understood. Efforts have been made to interpret the dynamical component of density fluctuation observed within narrow phase space intervals (local pattern) in AB interactions in terms of phenomena like (i) Bose-Einstein correlation, (ii) jet structure of particle emission, (iii) resonance decay, (iv) collective phenomena, (v) parton shower cascade mechanism and (vi) some exotic process like the thermal/non-thermal phase transition etc.. Various methods have been developed to characterize the dynamical component in terms of a small number

of well behaved parameters. A brief item-wise discussion on some of the statistical techniques used to study local density fluctuations of multiparticle production are summarily discussed below. Almost all of these issues will later be discussed in details with reference to the results obtained from the present investigation along with the corresponding physics analysis.

• **Intermittency:** The factorial moment of order q (a +ve integer) is defined as,

$$n^{[q]} = n(n-1)\cdots(n-q+1) \tag{1.76}$$

where n is the particle multiplicity in an arbitrary sub-interval (bin) of width say $\delta X = \Delta X/M$ of the variable X, ΔX being the overall domain of the variable under consideration which is divided into M non-overlapping equal sub-intervals. When properly normalized with respect to the average particle number per bin and averaged over a number of bins as well as over a large sample of events, the normalized factorial moment F_q scales with the phase space resolution size δX [78, 79]

$$F_q \propto \delta X^{-\phi_q} : \quad \delta X \to 0 \tag{1.77}$$

In multiparticle production physics the above relation for $\phi_q > 0$ is known as *intermittency*. The intermittency exponent ϕ_q used for characterizing turbulence in the theory of chaos to describe the development of a hydrodynamical system from a stable to a chaotic state, can analogously be used in particle production [80], and it can be determined from the asymptotic behavior of the scaling-law (1.77). For a *self-similar* density function F_q is found to follow such a scaling relation [78–80]. The technique first proposed by Bialas and Peschanski [78] to analyze a few high multiplicity JACEE events induced by high energy cosmic ray nuclei [81], has so far been extensively used to study local fluctuations of particle densities in high-energy collisions involving various combinations of target-projectile and collision energy (for review see refs. [82, 83]). In AB collisions the intermittency parameters may contain signatures of some kind of phase transition [84]. In view of self-similarity dominating the particle production process contradictory suggestions have also been made [85].

• **Cumulant Moment:** Evidence of genuine higher order particle correlations can be obtained only after subtracting their contribution originating from lower order(s). For this purpose one can study the *cumulant moments* (K_q) and the *oscillatory moments* (H_q). The F_q and the K_q moments are related by a recurrence relation

$$F_q = \sum_{j=1}^{q-1} \binom{q-1}{j-1} F_{q-j} K_j + K_q; \quad \text{for } q \geqslant 2. \tag{1.78}$$

H_q is now defined as the ratio $H_q = K_q/F_q$. According to a QCD parton shower cascade model [86] the H_q moments should oscillate with order number q about the $H_q = 0$ line. Almost all the correlation studies (just to cite a few of them [87–90]) have showed the validity of the α-model and some of them are also in agreement with the QCD based parton shower cascade model mentioned above [86].

• **Factorial Correlator:** While the SFM is used to look into the local (dynamical) density fluctuation, the the two-fold factorial moment or *factorial correlator* (FC) provides a bin-to-bin correlation of fluctuations within an event. Hence, the FC provides information on the dynamics of particle production beyond that obtained from single particle inclusive spectra. According to the α-model of particle production [79], factorial correlator (F_{pq}) calculated for two equal sized non-overlapping bins (say m-th and m'-th) separated by a distance D called the correlation length, defined as

$$F_{pq} = \frac{\left\langle n_m^{[q]}\, n_{m'}^{[q]} \right\rangle}{\left\langle n_m^{[q]} \right\rangle \left\langle n_{m'}^{[q]} \right\rangle} \tag{1.79}$$

depends only on D and not on δX. F_{pq} follows a scaling relation like

$$F_{pq} \sim D^{-\phi_{pq}}. \tag{1.80}$$

The exponent ϕ_{pq} measures the correlation length, and according to the α-model the exponent ϕ_{pq} is expected to follow a relation like, $\phi_{pq} = (p.q)\,\phi_{11}$.

• **Self-Affinity:** The effect of intermittency is more prominent in higher dimensions [91]. This is due to the fact that the actual process of multiparticle production takes place in a three dimensional space, and a dimensional reduction in the analysis reduces the extent of fluctuation. It is also very unlikely and the actual fact of matter is that the distribution of particles is not isotropic in all (longitudinal and transverse) directions. As a result, the scaling-law Eq. (1.77) for a self-similar partitioning of phase space is not found to be exact in higher dimensions. Hence, the scaling behavior should be different in different directions, and in a higher dimensional analysis a scaling behavior like Eq. (1.77) can be retrieved only by incorporating unequal partitioning in different directions. This is known as *self-affine* scaling. The self-affine structure of phase space is characterized by a 'roughness' parameter called the *Hurst exponent* (H) [92]. For $H = 1$ self-affine partitioning reduces to self-similar one. The anomalous scaling of two dimensional SFM in AB collisions was studied in detail by the EMU01 collaboration for different projectiles and different incident energies in emulsion experiments [93]. The EMU01 analysis showed that in order to recover the scaling-law (1.77) the phase space should be divided finer in the longitudinal η direction than in the transverse φ direction.

• **Erraticity:** The *erraticity moment* C_{pq} first introduced in ref. [94] to investigate both the spatial density fluctuations and the event-to-event fluctuations. The moment C_{pq} is analytically connected with a parameter called the *entropy index* μ_q, a direct measure of the degree of fluctuation in event space. μ_q is also a suitable parameter for measuring the chaotic behavior in the QCD branching process [95], possessing another advantage that it can identify whether a branching process is initiated by a quark or by a gluon. Erraticity analysis has been performed at various energies [96–98]. The experimental results are compared with Monte-Carlo simulations. The brief observations of the erraticity analysis are (i) the experimental values of the entropy indices in all cases are non-zero and significantly greater than the simulated values, (ii) the experimental results more or less agree with the theoretical predictions, (iii) μ_q decreases with increasing square-root of event multiplicity ($\sqrt{N_{ch}}$), and (iv) the pattern is independent of the energy involved in interactions [96]. In case of pp collisions it is also noticed that the reaction may not be triggered by the QCD parton cascading.

• **Multifractality:** A highly fluctuating signal can also be characterized in terms of the theory of fractals. For a self-similar object a *fractal dimension* can characterize the system, whereas an irregular or a multifractal object requires a set/spectrum of such dimensions. Multifractality is understood to be one probable cause of the observed density fluctuations in high-energy collisions. A multifractal analysis of multiparticle distribution data is based on evaluating *Hwa's moment* (or frequency moments) G_q [99, 100] and *Takagi's moment* T_q [101]. The G_q moment analysis is affected by the finiteness of event multiplicity ($\langle N_{ch} \rangle$). In this method the statistical noise can be eliminated by generating a random number based simulated event sample without invoking any inter-particle correlation. On the other hand, Takagi's moment is not influenced by the finiteness of $\langle N_{ch} \rangle$, but the mechanism of eliminating noise has not yet developed. Another very popular technique of dynamical time series data analysis, the so-called multifractal detrended fluctuation analysis (MF-DFA) [102], has recently been implemented for the multifractal characterization of high-energy AB collision data [103]. The MF-DFA method is not yet fully customized for the multiparticle data analysis and only a couple of articles are found in the literature where the MF-DFA method is used to analyzed the Au + Au collision data at 200A GeV [103, 104].

• **Azimuthal Structure:** In order to look into the nature of particle production in the azimuthal plane, one can use the prescription of ref. [105] which is known as the 'azimuthal structure analysis'. The objective of this analysis is to investigate whether the emitted particles prefer to come out in clusters (or subgroups) and if so, then whether the clusters are confined to narrow intervals of both longitudinal and transverse phase space variables i.e., *jet-like*, or confined only to a narrow interval of longitudinal variable but covers the entire allowed region of transverse one i.e., *ring-like*. The idea is based on a speculation that

either 'Cherenkov gluon emission' or a 'Mach shock wave' formation in nuclear/partonic medium [106] is responsible for such unusual structures. The EMU01 collaboration showed the presence of jet-like particle subgroups in ^{16}O and ^{32}S-induced interactions in nuclear emulsion experiments [105]. But the observation could be explained by the $\gamma \rightarrow e^-e^+$ conversion and interference between identical particles (HBT). In some other experiments however, presence of ring-like structure was observed [107–109].

• **Wavelet Analysis:** Wavelet transforms are a mathematical tool to perform signal analysis when signal frequency itself is a function of time. For certain classes of signals and images wavelet analysis provides more precise information about the signals. Recently, the technique has successfully been applied to analyze multiparticle emission data [110]. The wavelet analysis in high-energy collisions is based on the assumption that the dynamical fluctuation would be manifested by excess particles located at some characteristic position and at some characteristic resolution(s). Wavelet transform of a function of pseudorapidity say, $f(\eta)$ is given by [111]

$$W_\Psi(a,b)f(\eta) = \frac{1}{\sqrt{C_\Psi}} \int_{-\infty}^{+\infty} f(\eta)\Psi_{a,b}(\eta)d\eta, \tag{1.81}$$

where

$$\Psi_{a,b}(\eta) = a^{1/2}\Psi\left(\frac{\eta - b}{a}\right) \tag{1.82}$$

is called the mother wavelet, C_Ψ is a normalization constant. For continuous wavelets both the translation parameter b and the scale parameter a are continuous variables. The choice of a wavelet depends on the problem studied. Therefore, it is not unique. In multiparticle data analysis, the second derivative of the Gaussian function

$$g_2(x) = (1 - x^2)\exp(-x^2/2) \tag{1.83}$$

known as the 'Mexican hat' (MHAT), is usually chosen as the mother wavelet and the signal to be analyzed is the η-distribution. The irregularities are revealed in the wavelet pseudorapidity spectra within a particular scale region and they are interpreted as the preferred pseudorapidity values of the groups of emitted particles [107, 110]. Till date only a handful of results on wavelet analysis can be found in literature.

• **Void Analysis:** Multiparticle (rapidity) distributions in high-energy interactions exhibit both large spikes and deep valleys. From the perspective of underlying mechanism of multiparticle production both are equally important, and are complementary to each other. It is known that higher order cumulant correlation functions C_N can be constructed out of two-particle cumulant correlation functions C_2 [112]. Actually C_N is proportional to the product of $(N-1)$ two-particle reduced cumulants summed over all permutations.

This scheme successfully implemented in both galaxy-galaxy and particle-particle correlation studies, is formally termed as 'linked-pair ansatz' in multiparticle phenomenology. The technique is based on finding out a rapidity gap distribution $P_0(\Delta y)$ that measures the chance of finding out no particle within certain rapidity interval (Δy) [113]. Based on the hierarchical model of particle correlations stated above, it has been shown that a scaling behavior of the void probability distribution provides a sensible proof of the linked-pair approximation. The analysis method has so far been successfully tested in several high-energy experiments.

Bibliography

[1] D. J. Gross and F. Wilczek, *Phys. Rev. Lett.* **30**, 1343 (1973);
D. J. Gross and F. Wilczek, *Phys. Rev.* **D 8**, 3633 (1973).

[2] H. Politzer, *Phys. Rev. Lett.* **30**, 1346 (1973).

[3] S. Bethke, *Nucl. Phys. Proc.* **121** (Suppl.), 74 (2003).

[4] F. Karsch, E. Laemann and A. Peikart, *Nucl. Phys.* **B605**, 579 (2001).

[5] J. C. Collins and M. J. Perry, *Phys. Rev. Lett.* **34**, 1353 (1975);
N. Cabbibo and G. Parisi, *Phys. Lett.* **B 59**, 67 (1975).

[6] T. Banks and A. Casher, *Nucl. Phys.* **B 109**, 103 (1980).

[7] R. Hagedorn, *Nuovo Cim. Suppl.* **3**, 147 (1965)
R. hagedron and J. Rafelski, *Phys. Lett.* **B 97**, 136 (1980);
R. Hagedron, *Z. Phys.* **C 17**, 265 (1983).

[8] J. Berges, *Effective Theories of Matter (1)* (Lectures given at 11th Summer School and Symposium on Nuclear Physics, Seoul, Korea 1998) [arXiv:hep-ph/9902419].

[9] E. V. Shuryak, *Phys. Lett.* **B 78**, 150 (1978); *Phys. Rep.* **61**, 71 (1980).

[10] G. Chapline, M. Johnson, E. Teller *et al., Phys. Rev.* **D 8**, 4302 (1973).

[11] R. S. Bhalerao *Relativistic heavy-ion collisions* (Lectures given at the First Asia-Europe-Pacific School of High-Energy Physics, Japan, 2012) [arXiv:1404.3294v1].

[12] K. Adcox *et al.* (PHENIX Collaboration), *Nucl. Phys.* **A 757**, 184 (2005).

[13] P. Barun-Munzinger and J. Stachel, *Nature* **448**, 302 (2007).

[14] F. Karsch, *Nucl. Phys.* **A 698**, 199c (2002).

[15] M. Kliemant, R. Sahoo, T. Schuster and R. Stock, *Lect. Not. Phys.* **785**, 23 (2010) in *The Physics of the Quark-Gluon Plasma: Introductory Lectures*, Eds. S. Sarkar, S. Satz and B. Sinha, (Springer-Verlag, Berlin, Germany, 2010).

[16] N. Herrmann *et al., Ann. Rev. Nucl. Part. Sci.* **49**, 581 (1999).

[17] J. Adams *et al.* (STAR Collaboration), *Nucl. Phys.* **A 757**, 102 (2005).

[18] J. Letessier and J. Rafelski, *Hadrons and Quark-Gluon Plasma*, (Cambridge University Press, Cambridge, UK, 2004).

[19] J. D. Bjorken, *Phys. Rev.* **D 27**, 140 (1983).

[20] I. S. Hughes, *Elementary particles*, (Cambridge University Press, UK, 1991).

[21] B. Friman, C. Höhne, J. Knoll, S. Leupold, J. Randrup, R. Rapp and P. Senger (Eds.), *The CBM Physics Book* (Springer, 2010).

[22] H. Schopper and Luigi D. Lella (Eds.), *60 Years of CERN Experiments and Discoveries* (World Scientific Publishing Company, 2015).

[23] M. J. Tannenbaum, arXiv:1201.5900[nucl-ex] (2012).

[24] J. Rak and M. J. Tannenbaum, *High-p_T Physics in the Heavy Ion Era* (Cambridge University Press, Cambridge, UK, 2013).

[25] I. Arsene *et al.* (BRAHMS Collaboration), *Nucl. Phys.* **A 757**, 1 (2005).

[26] B. B. Back *et al.* (PHOBOS Collaboration), *Nucl. Phys.* **A 757**, 28 (2005).

[27] D. Rischke and G. Levin, *Nucl. Phys.* **A 750**, 1 (2005).

[28] Press Conference, *A New State of Matter Created at CERN*, http://newstate-matter.web.cern.ch/newstate-matter/Story.html

[29] R. Vogt, *Ultrarelativistic Heavy-Ion Collisions*, (Elsevier, Amsterdam, The Netherlands, 2007).

[30] F. Karsch and E. Laermann, *Quark-Gluon Plasma*, Eds. R. C. Hwa and X. N. Wang, (World Scientific, Singapore, 2003).

[31] E. Fermi, *Prog. Theo. Phys.*, **5**, 570 (1950); *ibid* **81**, 683 (1951).

[32] L. D. Landau, *Izv. Akad. Nauk., Ser. Fiz.* **17**, 51 (1953);
S. Z. Belensky and L. D. Landau *Ups. Fiz. Nauk.* **56**, 309 (1955).

[33] E. K. G. Sarkisyan and A. S. Sakharov, *Eur. Phys. J.* **C 70**, 533 (2010);
A. N. Mishra, R. Sahoo, E. K. G. Sarkisyan and A. S. Sakharov, *Eur. Phys. J.* **C 74**, 3147 (2014).

[34] P. Kolb and U. Heinz, *Quark-Gluon Plasma 3*, Eds., R. C. Hwa and X. N. Wang (World Scientific, Singapore, 2003).

[35] K. Yagi, T. Hatsuda and Y. Miake, *Quark-Gluon Plasma, From Big Bang to Little Bang* (Cambridge University Press, Cambridge, UK 2005).

[36] C. Y. Wong, *Introduction to High-Energy Heavy-Ion Collisions* (World Scientific, 1994).

[37] L. D. McLerran *et al., Phys. Lett.* **B 98**, 195 (1981); *Phys. Rev.* **D 24**, 450 (1981);
J. Kuti, J. Polonyi and K. Szlachanyi, *Phys. Lett.* **B 98**, 199 (1981).

[38] H. Satz, Extreme States of Matters in Strong Interaction Physics, *Lect. Not. Phys.* **841**, 111 (Springer-Verlag Berlin Heidelberg, 2012);
A. Ayala *et al., Nucl. Phys.* **B 897**, 77 (2015).

[39] B. Müller and J. L. Nagle, *Ann. Rev. Nucl. Part. Phys.* **56**, 93 (2006).

[40] J. W. Harris and B. Müller, *Ann. Rev. Nucl. Part. Sci.* **46**, 71 (1996).

[41] G. Goldhaber *et al. Phys. Rev.* **120**, 300 (1960).

[42] U. A. Wiedemann and U. W. Heinz, *Phys. Rept.* **319**, 145 (1999).

[43] R. Hanbury-Brown and R. Q. Twiss, *Nature 178*, 1046 (1956).

[44] U. A. Wiedemann, *Nucl. Phys.* **A 661**, 65 (1999).

[45] H. A. Gustafsson *et al.*, *Phys. Rev. Lett.* **52**, 1590 (1984).

[46] J.-Y. Ollitrault, *Phys. Rev.* **D 46**, 229 (1992).

[47] K. H. Ackermann *et al.* (STAR Collaboration), *Phys. Rev. Lett.* **86**, 402 (2001).

[48] C. Adler *et al.* (STAR Collaboration), *Phys. Rev. Lett.* **87**, 182301 (2001).

[49] B. Mohanty and J. Serreau, *Phys. Rept.* **414**, 263 (2005).

[50] T. K. Nayak, *J. Phys.* **G 32**, S187 (2006).

[51] V. Koch, M. Bleicher and S. Jeon, *Nucl. Phys.* **A698**, 261 (2002).

[52] J. Rafelski, B. Muller, *Phys. Rev. Lett.* **48**, 1066 (1982) [Erra. *ibid* **56**, 2334 (1986)];
P. Koch, B. Muller and J. Rafelski, *Phys. Rep.* **142** (1986).

[53] B. Sinha, *Phys. Lett.* **B 135**, 169 (1984).

[54] P. Koch, B. Muller and J. Rafelski, *Z. Phys.* **A 324**, 453 (1986).

[55] V. Koch, *Acta Phys. Polon.* **B 29**, 3233 (1998).

[56] P. Aurenche, arXiv:hep-ph/0201011; F. Arleo *et al.*, *"Photon physics" section*, CERN Yellow Report, 2004-009, arXiv:hep-ph/0311131 (2007).

[57] T. Peitzmann and M. H. Thoma, *Phys. Rep.* **364**, 175 (2002);
D. Boyanovsky and H. J. de Vega, *Phys. Rev.* **D 68**, 065018 (2003);
F.-M. Liu and K. Werner, *Phys. Rev. Lett.* **106**, 242301 (2011);
M. Wilde *et al.* (ALICE collaboration), *Nucl. Phys.* **A 904**, 573c (2013).

[58] K. Kanaya and H. Satz, *Phys. Rev.* **D 34**, 3193 (1986);
T. A. DeGrand and C. E. DeTar, *Phys. Rev.* **D 34**, 2469 (1986).

[59] T. Matsui and H. Satz, *Phys. Lett.* **B 178**, 416 (1986).

[60] A. Adare *et al.* (PHENIX Collaboration), *Phys. Rev. Lett.* **98**, 232301 (2007).

[61] P. Pillot (for the ALICE collaboration), *J. Phys.* **G 38**, 124111 (2011);
A. Grelli (for the ALICE collaboration), *J. Phys.* **G 316**, 012025c (2011).

[62] J. D. Bjorken, Preprint FERMILAB-PUB-82-059-THY (1982);
K. Adcox (for the PHENIX Collaboration), *Nucl. Phys.* **A 757**, 184 (2005);
K. Aamodt *et al.,* (ALICE Collaboration) *Phys. Lett.* **B 696**, 30 (2011);
S. Chatrchyan *et al.* (CMS Collaboration), *Eur. Phys. J.* **C 72**, 1945 (2012).

[63] H. Sorge, *Phys. Rev. Lett.* **78**, 2309 (1997); *Phys. Lett.* **B 402**, 251 (1997).

[64] H. Bebie, P. Gerber, J. L. Goity and H. Leutwyler, *Nucl. Phys.* **B 378**, 95 (1992).

[65] S. A. Bass *et al., Prog. Nucl. Part. Phys.* **41**, 255 (1998);
M. Bleicher *et al., J. Phys.* **G 25**, 1859 (1999).

[66] B. Andersson, G. Gustafson and B. Nilsson-Alqmvist, *Nucl. Phys.* **B 281**, 289 (1987);
B. Nilsson-Alqmvist and E. Stenlund, *Comp. Phys. Commun.* **43**, 387 (1987).

[67] X. N. Wang and M. Gyulassy, *Phys. Rev.* **D 44**, 3501 (1991).

[68] A. Capella, U. Sukhatme and J. Tran Thanh Van, *Z. Phys.* **C 3**, 329 (1980);
J. Ranft, *Phys. Rev.* **D 37**, 1842 (1988).

[69] T. Sjöstrand, M. van Zijil, *Phys. Rev.* **D 36**, 2019 (1987).

[70] Z.-W. Lin, C. M. Ko, B.-A. Li, B. Zhang, S. Pal, Phys. Rev. C 72, 064901 (2005).

[71] B. Zhang, *Comp. Phys. Commun.* **109**, 193 (1998).

[72] T. Sjöstrand, *Comp. Phys. Commun.* **82**, 74 (1994).

[73] B. A. Li and C. M. Ko, *Phys. Rev.* **C 52**, 2037 (1995).

[74] Zi-Wei Lin and C. M. Ko, *Phys. Rev.* **C 65**, 034904 (2002).

[75] N. Xu and M. Kaneta, *Nucl. Phys.* **A 698**, 306 (2002).

[76] A. Andronic, P. Braun-Munzinger and J. Stachel, *Nucl. Phys.* **A 772**, 167 (2006).

[77] J. Cleymans, H. Oeschler, K. Redlich and S. Wheaton, *J. Phys.* **G 32**, S165 (2006).

[78] A. Bialas and R. Peschanski, *Nucl. Phys.* **B 273**, 703 (1986).

[79] A. Bialas and R. Peschanski, *Nucl. Phys.* **B 308**, 857 (1988).

[80] P. Carruthers *et al.*, *Phys. Lett.* **B 222**, 487 (1989).

[81] T.H. Burnett *et al.* (JACEE Collaboration), *Phys. Rev. Lett.* **50**, 2062 (1962).

[82] W. Kittel and E. A. De Wolf, *Soft Multihadron Dynamics* (World Scientific, 1995).

[83] E. A. De Wolf, I. M. Dremin and W. Kittel, *Phys. Rep.* **270** 1 (1996).

[84] A. Bialas and R. C. Hwa, *Phys. Lett.* **B 253**, 436 (1991).

[85] R. C. Hwa (Ed.), *Quark-Gluon Plasma* (World Scientific, Singapore, 1990).

[86] I. M. Dremin, *Phys. Lett.* **B 313**, 209 (1993).

[87] M. I. Adamovich *et al.* (EMU01 Collaboration), *Nucl. Phys.* **B 388**, 3 (1992).

[88] D. Ghosh *et al.*, *Phys. Rev.* **C 52**, 2092 (1995).

[89] M. K. Ghosh *et. al.*, *J. Phys.* **G 34**, 177 (2007).

[90] S. Islam and R. Hassan, *J. Phys.* **G 34**, 779 (2007).

[91] W. Ochs, *Phys. Lett.* **B 247**, 101 (1990); *Z. Phys.* **C 50**, 339 (1991).

[92] L. Liu, Y. Zhang, Y. Wu, *Z. Phys.* **C 69**, 323 (1996).

[93] M. I. Adamovich *et al.* (EMU01 Collaboration), *Z. Phys.* **C 76**, 659 (1991).

[94] Z. Cao and R. C. Hwa, *Phys. Rev. Lett.* **75**, 1268 (1995); *Phys. Rev.* **D 53**, 6608 (1996); *Phys. Rev.* **E 56**, 326 (1997).

[95] A. Altarelli and G. Parisi, *Nucl. Phys.* **B 216**, 298 (1977).

[96] W. Shaoshun and W. Zhaomin, *Phys. Rev.* **D 57**, 3036 (1998).

[97] R. Hassan *et al., J. Phys.* **G 28**, 2939 (2002).

[98] D. Chanda *et al., Phys. Rev.* **C 71**, 034904 (2005).

[99] R. C. Hwa, *Phys. Rev.* **D 41**, 1456 (1990).

[100] C. B. Chiu and R. C. Hwa, *Phys. Rev.* **D 43**, 100 (1991).

[101] F. Takagi, *Phys. Rev. Lett.* **72** 32 (1994).

[102] J. W. Kantelhardta *et al., Physica* **A 316** 87 (2002).

[103] Y. X. Zhang, W. Y. Qian and C. B. Yang, *Int. J. Mod. Phys.* **A 23**(18), 2809 (2007).

[104] X. Wang and C. B. Yang, *Int. J. Mod. Phys. E* **22**(4), 1350021 (2013).

[105] M. I. Adamovich *et al.* (EMU01 Collaboration), *J. Phys.* **G 19**, 2035 (1993).

[106] I. M. Dremin, *Pis'ma Zh. Eksp. Teor. Fiz.* **30**, 152 (1979); *Yad. Fiz.* **33**, 1357 (1981).

[107] I. M. Dremin *et al., Phys. Lett.* **B 499**, 97 (2001).

[108] S. Vokál *et al., Phys. Atom. Nucl.* **71**, 1395 (2008).

[109] S. Vokál *et al., Phys. Atom. Nucl.* **72**, 237 (2009).

[110] V. V. Uzhinsky *et al., Phys. Atom. Nucl.* **67**, 156 (2004).

[111] I. Daubechies, *Ten Lectures on Wavelets* (Society for Industrial and Applied Mathematics, Philadelphia, Pennsylvania, 1992).

[112] P. Carruthers and I. Sarcevic, *Phys. Rev. Lett.* **63**, 1562 (1989).

[113] S. Hegyi, *Phys. Letts.* **B 274**, 214 (1992); *Phys. Letts.* **B 309**, 443 (1993).